1-16-2020

# K2 observations of the pulsating subdwarf B stars UY Sex and V1405 Ori

Michael D. Reed
*Missouri State University*

M. Yeager
*MSU Underraduate*

J. Vos

J. H. Telting

R. H. Ostensen

*See next page for additional authors*



## Recommended Citation

Reed, M. D., M. Yeager, J. Vos, J. H. Telting, R. H. Østensen, A. Slayton, A. S. Baran, and C. S. Jeffery. "K2 observations of the pulsating subdwarf B stars UY Sex and V1405 Ori." Monthly Notices of the Royal Astronomical Society 492, no. 4 (2020): 5202-5217.

Monthly Notices
of the
ROYAL ASTRONOMICAL SOCIETY

MNRAS **492,** 5202–5217 (2020)
Advance Access publication 2020 January 16

doi:10.1093/mnras/staa144

# K2 observations of the pulsating subdwarf B stars UY Sex and V1405 Ori

M. D. Reed [1]★ M. Yeager,[1] J. Vos,[2] J. H. Telting,[3] R. H. Østensen,[1] A. Slayton,[1] A. S. Baran [1,4] and C. S. Jeffery [5]

[1]*Department of Physics, Astronomy and Materials Science, Missouri State University, 901 S. National, Springfield, MO 65897, USA*
[2]*Instituto de Física y Astronomía y Centro de Astrofísica de Valparaíso, Chile*
[3]*Nordic Optical Telescope, Rambla José Ana Fernández Pérez 7, E-38711 Breña Baja, Spain*
[4]*ARDASTELLA Research Group, Institute of Physics, Pedagogical University of Cracow, ul. Podchorąży ch 2,30-084 Kraków, Poland*
[5]*Armagh Observatory and Planetarium, College Hill, Armagh BT61 9DG, UK*

Accepted 2020 January 14. Received 2020 January 13; in original form 2019 October 23

## ABSTRACT

We processed and analysed K2 observations of the pulsating subdwarf-B (sdBV) stars UY Sex and V1405 Ori. We detect 97 p-mode pulsations in UY Sex while we discover V1405 Ori to be a rare rich hybrid pulsator with over 100 p-mode pulsations and 19 g-mode pulsations. We detect frequency multiplets, which we use to identify pulsation modes as well as determine rotation periods. For UY Sex, we find a rotation period of the envelope of 24.6 ± 3.5 d and for V1405 Ori, we find a rotation period of 0.555 ± 0.029 d for the p modes and a marginal detection of 4.2 ± 0.4 d for the g modes. We discover that V1405 Ori is unique among sdBV stars observed to date. It is a rich hybrid pulsator, allowing us to simultaneously probe the envelope and interior; its frequency multiplets indicate V1405 Ori to be rotating differentially with the core rotating more slowly than the envelope, and it is also in a short-period binary (0.398 d) with an envelope that is nearly but not quite tidally locked. For both stars, we have obtained spectroscopic follow-up observations and examine combining them with *Gaia* parallaxes and archival photometry to determine fundamental properties. Our derived masses are inconsistent with spectroscopy and previous determinations and indicate problems with the methodology.

**Key words:** stars: oscillations – subdwarfs.

## 1 INTRODUCTION

Subdwarf-B (sdB) stars are helium-burning stars with thin hydrogen envelopes located on the extreme horizontal branch. Typical sdB stars are $\sim 0.5\,M_\odot$ with an envelope mass of $< 0.01\,M_\odot$, $5.0 < \log g/\mathrm{cm\,s^{-2}} < 5.8$, $0.15 < R < 0.35\,R_\odot$, and $20\,000 < T_{\rm eff} < 40\,000$, K (Heber 2016). It was discovered in 1996 that some sdB stars were variable (sdBV), termed V361 Hya stars (Kilkenny et al. 1997). V361 Hya stars are pressure (p)-mode pulsators with periods of ≤15 min and tend to be hotter sdB stars. The other class of sdBV stars was discovered in 2003, termed V1093 Her stars, which have gravity (g)-mode pulsations with typical periods >45 min and tend to be on the cooler end of sdB stars (Green et al. 2003). The first theoretical pulsation model for sdBV stars was published by Charpinet et al. (1997), with the models being updated and revised as new observational data become available (Constantino et al. 2015; Ghasemi et al. 2017).

With the discovery of sdB variability, asteroseismic analyses were now possible, giving observational constraints to internal modelling of these stars. Non-radial pulsations can be characterized by three quantum numbers, $n$ (radial order), $\ell$ (degree), and $m$ (azimuthal order). Mode identification from photometry is primarily accomplished through two methods, the analysis of asymptotic overtone spacing of g-mode pulsations (Reed et al. 2011) and of rotationally induced frequency multiplets (Baran et al. 2012) in both p and g modes. As g-mode pulsations probe deeper into the star, a smooth asymptotic period spacing sequence indicates smooth transitions between chemical compositions within the star, while trapped modes (Østensen et al. 2014) indicate sharper transition zones that modify pulsations in the resonant cavity of the star (Heber 2016). Frequency multiplets can measure the rotation period of the star, which is especially useful in the case of binary systems and hybrid pulsators. While not in the asymptotic regime, p-mode overtone spacings can also be compared to models, which predict spacings of 800–1200 μHz (Charpinet et al. 2002). The best case so far (Baran et al. 2012) shows smaller spacings while some others have spacings commensurate with models (Foster et al. 2015). Stochastic features of pulsations can also be used to probe mode stability (Østensen et al. 2014). Hybrid pulsators that have both p and g modes can be used to determine differential rotation between the core and the envelope of the star, with p modes occurring only in

★ E-mail: mikereed@missouristate.edu

**Table 1.** Frequency list for UY Sex. Column 1 provides an identifier, column 2 the fitted frequency, column 3 the amplitude, and column 4 the corresponding signal to noise. Column 5 provides our mode ID and column 6 lists frequencies also found in a: Billères et al. (1997), b: O'Donoghue et al. (1998), c: Kilkenny et al. (2002a), and/or d: Charpinet et al. (2003, including mode degree from their Fig. 3).

| ID | Freq (μHz) | Amp (ppt) | S/N | $\ell$, $m$ | $f_{a,b,c}$ |
|---|---|---|---|---|---|
| f1 | 2010.434 (3) | 0.06 (2) | 8.90 | | |
| f2 | 3052.843 (6) | 0.15 (1) | 21.84 | | |
| f3 | 3509.287 (10) | 0.09 (1) | 12.79 | | |
| f4 | 4240.341 (21) | 0.04 (1) | 5.83 | | |
| f5 | 4294.101 (13) | 0.06 (1) | 9.18 | | |
| f6 | 4867.708 (55) | 0.04 (2) | 5.10 | | |
| f7 | 5204.000 (26) | 0.04 (1) | 5.32 | 1, −1 | |
| f8 | 5204.620 (29) | 0.04 (1) | 5.31 | 1, 0 | |
| f9 | 5700.206 (5) | 0.36 (2) | 51.22 | | c, d2 |
| f10 | 5966.248 (21) | 0.04 (1) | 5.83 | | |
| f11 | 6104.664 (8) | 0.10 (1) | 14.40 | | |
| f12 | 6126.342 (6) | 0.34 (2) | 48.76 | 1, −1 | c, d3 |
| f13 | 6126.694 (4) | 0.47 (2) | 67.22 | 1, 0 | |
| f14 | 6177.652 (1) | 1.56 (2) | 222.90 | | a, b, c |
| f15 | 6269.820 (13) | 0.08 (1) | 10.89 | 1, −1 | |
| f16 | 6270.270 (23) | 0.04 (1) | 6.31 | 1, 0 | |
| f17 | 6270.680 (20) | 0.05 (1) | 6.78 | 1, 1 | |
| f18 | 6405.214 (181) | 0.68 (2) | 97.31 | | |
| f19 | 6405.780 (134) | 0.60 (2) | 85.86 | | |
| f20 | 6406.420 (139) | 0.91 (2) | 130.22 | | |
| f21 | 6406.839 (136) | 0.09 (2) | 12.45 | | |
| f22 | 6407.248 (135) | 0.42 (2) | 60.10 | | |
| f23 | 6638.580 (17) | 0.06 (1) | 9.23 | 4, −1 | |
| f24 | 6638.940 (7) | 0.17 (1) | 24.47 | 4, 0 | |
| f25 | 6639.280 (7) | 0.17 (1) | 24.04 | 4, 4 | c |
| f26 | 6640.870 (10) | 0.11 (1) | 15.74 | 3, −1 | |
| f27 | 6641.390 (11) | 0.12 (1) | 16.60 | 3, 0 | |
| f28 | 6642.530 (10) | 0.10 (1) | 14.88 | 3, 2 | |
| f29 | 6643.440 (7) | 0.18 (1) | 25.04 | 3, 3 | |
| f30 | 6824.1 (3.7) | stoch | | | c |
| f31 | 6887.039 (0) | 4.34 (2) | 620.69 | | a, b, c, d0 |
| f32 | 6950.2 (1.5) | stoch | | | |
| f33 | 7015.984 (15) | 0.13 (2) | 18.29 | 3, −3 | |
| f34 | 7017.359 (5) | 0.40 (2) | 57.10 | 3, 0 | c |
| f35[a] | 7018.280 (170) | 0.16 | 22.90 | 3, 2 | |
| f36 | 7021.950 (150) | 0.57 | 81.57 | 3, −2 | |
| f37 | 7022.335 (79) | 0.51 | 72.98 | 3, −1 | |
| f38 | 7022.778 (1) | 1.36 (2) | 194.66 | 3, 0 | b, c, d1 |
| f39[a] | 7023.985 (223) | 0.24 | 34.77 | 3, 3 | |
| f40 | 7029.789 (13) | 0.15 (2) | 21.67 | | b |
| f41 | 7038.163 (0) | 4.89 (2) | 700.10 | 2, −2 | a, b, c, d2 |
| f42 | 7039.199 (1) | 1.48 (2) | 212.28 | 2, 0 | c |
| f43 | 7040.106 (2) | 0.42 (1) | 59.70 | 2, 2 | c |
| f44 | 7052.787 (9) | 0.10 (1) | 13.63 | | |
| f45 | 7055.750 (16) | 0.07 (1) | 9.44 | | |
| f46[a] | 7130.270 (250) | 0.11 | 15.84 | 4, −1 | |
| f47 | 7131.271 (3) | 0.28 (1) | 39.67 | 4, 0 | c, d3 |
| f48 | 7132.220 (270) | 0.19 | 26.75 | 4, 2 | |
| f49 | 7133.071 (9) | 0.09 (1) | 13.05 | 4, 4 | |
| f50 | 7136.710 (12) | 0.07 (1) | 10.34 | 3, −3 | |
| f51 | 7138.026 (2) | 0.41 (1) | 59.31 | 3, 0 | c, d4 |
| f52 | 7139.166 (3) | 0.32 (1) | 45.64 | 3, 2 | |
| f53 | 7281.5 (1.8) | stoch | | | |
| f54 | 7315.505 (2) | 1.25 (2) | 179.21 | 1, 0 | c |
| f55 | 7316.102 (2) | 1.06 (3) | 151.69 | 1, 1 | b, c, d0 |
| f56 | 7502.292 (5) | 0.16 (1) | 23.08 | | b, c, d1 |
| f57 | 7509.1 (2.2) | stoch | | | |
| f58[a] | 8230.169 (80) | 0.09 | 12.45 | 2, −1 | |
| f59[a] | 8230.728 (144) | 0.13 | 19.03 | 2, 0 | c, d2 |
| f60[a] | 8231.222 (91) | 0.24 | 34.92 | 2, 1 | |
| f61 | 8231.790 (81) | 0.07 | 9.59 | 2, 2 | |
| f62 | 8280.469 (241) | 0.08 | 11.31 | | |
| f63 | 8662.9 (1.6) | stoch | | | d3 |
| f64 | 8928.226 (1) | 0.45 (3) | 64.31 | 2, −2 | |
| f65 | 8928.774 (1) | 0.38 (3) | 54.52 | 2, −1 | |
| f66 | 8929.304 (1) | 0.43 (3) | 61.68 | 2, 0 | a, b |
| f67 | 8930.180 (2) | 0.28 (3) | 39.64 | 2, 2 | |
| f68 | 9092.490 (9) | 0.09 (1) | 13.01 | | |
| f69 | 9097.367 (6) | 0.15 (1) | 20.88 | 1, −1 | d1 |
| f70 | 9097.808 (73) | 0.17 | 23.76 | 1, 0 | |
| f71 | 9581.567 (147) | 0.08 | 11.02 | 1, −1 | |
| f72 | 9582.088 (223) | 0.08 | 11.88 | 1, 0 | |
| f73 | 9599.680 (15) | 0.07 (1) | 9.80 | 6, −6/2, −2 | b |
| f74 | 9600.660 (10) | 0.11 (1) | 15.17 | 6, −4/2, 0 | |
| f75 | 9601.300 (9) | 0.12 (1) | 17.46 | 6, −3/2, 1 | |
| f76 | 9601.780 (8) | 0.14 (1) | 19.61 | 6, −2/2, 2 | c, d3 |
| f77 | 9602.110 (10) | 0.10 (1) | 14.74 | 6, −1/3, −2 | |
| f78 | 9603.140 (13) | 0.08 (1) | 11.85 | 6, 1/3, −1 | |
| f79 | 9603.690 (8) | 0.13 (1) | 18.46 | 6, 2/3, 0 | |
| f80 | 9604.100 (13) | 0.08 (1) | 11.46 | 6, 3/3, 1 | |
| f81 | 9604.550 (10) | 0.11 (1) | 15.46 | 6, 4/3, 2 | |
| f82 | 9605.170 (4) | 0.25 (1) | 36.06 | 6, 5/3, 3 | a, c |
| f83 | 9616.9 (0.7) | stoch | | | |
| f84 | 9647.5 (1.7) | stoch | | | |
| f85 | 9677.659 (2) | 1.13 (3) | 162.19 | | |
| f86 | 9867.124 (6) | 0.14 (1) | 19.87 | | |
| f87 | 9933.976 (16) | 0.06 (1) | 9.20 | | |
| f88 | 9935.150 (11) | 0.09 (1) | 13.52 | | |
| f89 | 9937.680 (13) | 0.08 (1) | 11.33 | | d0 |
| f90 | 10350.210 (15) | 0.08 (1) | 12.01 | | |
| f91 | 10353.860 (7) | 0.15 (1) | 21.18 | 1, −1 | d3 |
| f92 | 10354.270 (7) | 0.16 (1) | 22.18 | 1, 0 | |
| f93 | 11381.958 (28) | 0.03 (1) | 4.48 | 1, −1 | |
| f94 | 11382.397 (26) | 0.04 (1) | 5.23 | 1, 0 | |
| f95 | 11382.754 (17) | 0.05 (1) | 7.76 | 1, 1 | d0 |
| f96 | 12542.731 (32) | 0.06 (2) | 8.62 | | |
| f97 | 12723.027 (24) | 0.04 (1) | 5.12 | | |

*Note.* [a]These frequencies were fitted with Lorentzians as NLLS fitting would not converge to a solution. Regions that we interpret as stochastic in nature are labelled as such in the amplitude column.

the envelope and g modes probing the interior of the star. Six such hybrid pulsators have been analysed with the result that three spin as solid body rotators (Baran et al. 2012; Kern et al. 2018; Reed et al. 2019) and three rotate differentially (Foster et al. 2015; Baran et al. 2017; Reed et al. 2019), with the core rotating slower than the envelope.

While the Kepler mission's primary objective was to search for Earth-sized exoplanets, its observations have greatly advanced the study of sdBV stars. Kepler's long duration and high-duty cycle observations provide high-quality data and allow for the resolution of long-period g-mode pulsations, which have been unresolvable from the ground due to observational constraints. This paper will utilize 58.8-s short-cadence observations from the Kepler K2 mission, which observed in 80 d fields along the ecliptic plane, to further characterize two previously known p-mode sdBV stars.

In this paper, we apply asteroseismic techniques to the sdBV star UY Sex (also EPIC 248411044 and PG 1047+003), which has $K_p$ = 13.6 and V1405 Ori (also EPIC 246683636 and

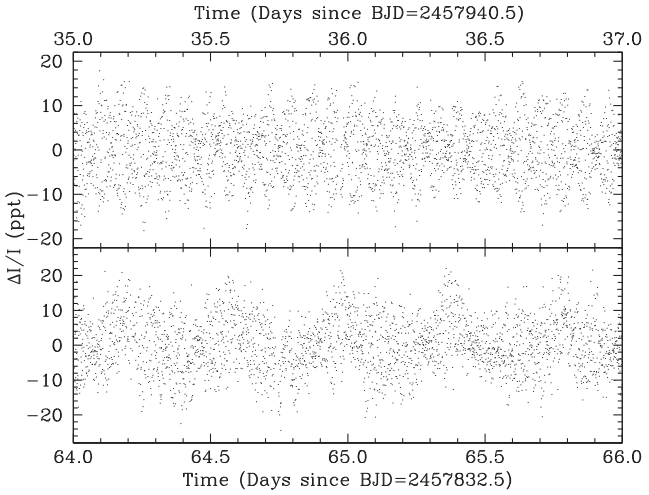


**Figure 1.** Sample light curves of UY Sex (top) and V1405 Ori (bottom) showing a 2-d span. That of UY Sex is dominated by pulsations while V1405 Ori's is dominated by binarity.

KUV 04421+1416), which has $K_p = 15.1$. These stars were part of our K2 Guest Observer program, and we have previously published nine papers about K2-discovered sdBV stars (Baran et al. 2017, 2018; Jeffery et al. 2017; Ketzer et al. 2017; Baran et al. 2019; Silvotti et al. 2019; Reed et al. 2018, 2019, 2016). The two stars of this paper were known to have p-mode pulsations prior to K2 observations and we show how K2 observations reveal more seismic information than even multisite ground-based observations.

UY Sex was discovered to pulsate by Billères et al. (1997), who found five p-mode frequencies from 6000 to 9600 μHz with evidence for more frequencies. They provide atmospheric parameters of $T_{\rm eff} = 34,370\,K$ and $\log g/{\rm cm\,s^{-2}} = 5.7$. Other ground-based observations were obtained by O'Donoghue et al. (1998) and Kilkenny et al. (2002a). The former obtained data on 12 nights, found nine total frequencies in the same range as Billères et al. (1997), and determined $T_{\rm eff} = 35\,000 \pm 1000$ K and $\log g/{\rm cm\,s^{-2}} = 5.9 \pm 0.1$ from high signal-to-noise (S/N) spectroscopy. The latter was a four-site campaign of UY Sex spanning two weeks during 1998 using four telescopes that collected 98 hours of data with a 30 per cent duty cycle. The nine previous frequencies were verified, with nine additional detections. Out of these 18 frequencies, 11 were found to be parts of multiplets, with a triplet and a doublet having splittings of 1.05 μHz, and three other doublets spaced at integer multiples of 1.05 μHz, perhaps for higher degree ($\ell \geq 2$) modes. Assuming that the multiplets are rotationally induced, Kilkenny et al. (2002a) estimated a rotation period of 11.0 d. The presence of multiplets using ground-based data is rare, making UY Sex a promising candidate for analysis using K2 data. Charpinet, Fontaine & Brassard (2003) matched a seismic model for the periods and spectroscopic constraints of UY Sex and determined $M = 0.490 \pm 0.014\,{\rm M}_\odot$, $R = 0.136 \pm 0.003\,{\rm R}_\odot$, $L = 22.7 \pm 5.3$ ${\rm L}_\odot$, $\log g/{\rm cm\,s^{-2}} = 5.800 \pm 0.006$, and $T_{\rm eff} = 33\,000 \pm 1600$ K. They also (neglecting multiplets) associated modes with periods, which we provide (interpreted from their Fig. 3) in Table 1.

V1405 Ori was discovered to pulsate by Koen et al. (1999), who detected seven frequencies using data with a temporal resolution of ∼2.3 μHz and a $4\sigma$ detection limit of 2.5 parts-per-thousand (ppt). Follow-up observations by Reed et al. (2010) with an improved $4\sigma$ detection limit of 0.42 ppt (but essentially the same frequency

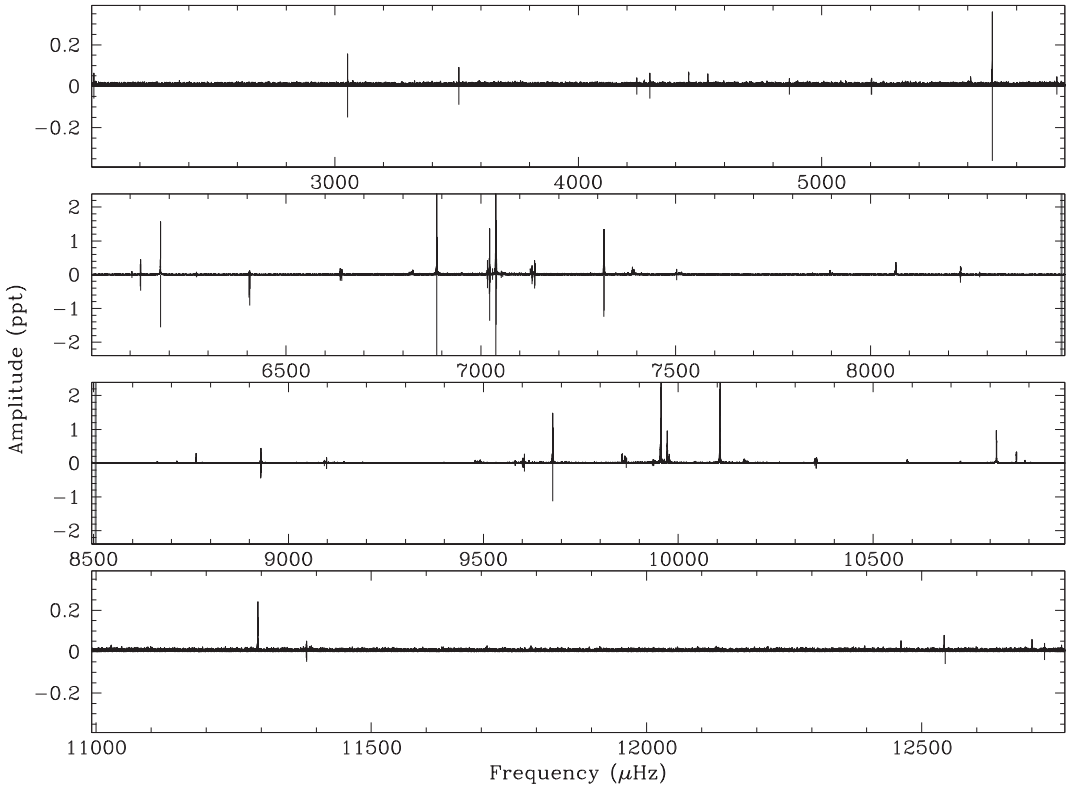


**Figure 2.** Fourier transform of UY Sex with peaks considered intrinsic to the star schematically mirrored below each panel. Most of the extrinsic peaks are caused by aliasing across the Nyquist frequency while some others are known spacecraft artefacts. The red line indicates the Nyquist frequency.

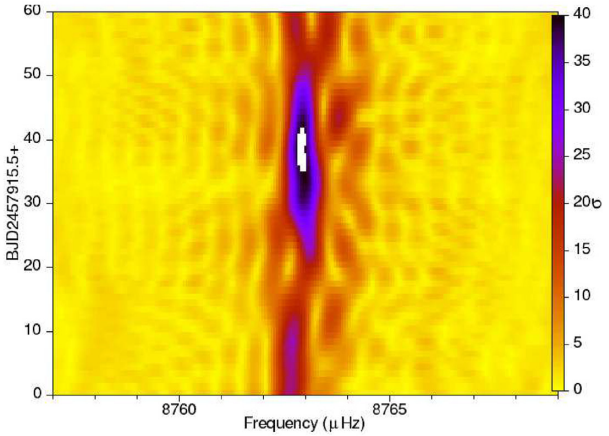


**Figure 3.** Sliding FT of UY Sex showing variations in amplitude and frequency. Colour scale is on the right. Note that red regions are above $5\sigma$.

resolution as Koen et al. 1999) detected 18 pulsation frequencies and discovered V1405 Ori to be in a reflection effect binary with an M-dwarf companion. The binary period was determined to be 0.398 d. Neither pulsation analyses produced mode identifications, though Reed et al. (2010) determined that frequency density required $\ell \geq 3$. Reed et al. (2010) also report spectroscopic follow-up data, which obtained nine spectra, measured $K = 90 \pm 5\,\mathrm{km\,s^{-1}}$, and derived a minimum companion mass of $0.25\,\mathrm{M_\odot}$, assuming a canonical sdB mass of $0.47\,\mathrm{M_\odot}$. Geier et al. (2014) obtained 14 spectra, finding very similar results of $K = 85.1 \pm 8.6\,\mathrm{km\,s^{-1}}$ and a minimum companion mass of $0.26\,\mathrm{M_\odot}$. They also determined $T_{\rm eff} = 35\,100 \pm 800$ K, $\log g/\mathrm{cm\,s^{-2}} = 5.66 \pm 0.11$, and $\log y = -2.5 \pm 0.2$.

## 2 K2 OBSERVATIONS AND ANALYSES

K2 campaigns span roughly 80 d. Our custom data processing, described in Baran et al. (2017), was used to extract fluxes from short-cadence image pixel files and produce pixel-flux decorrelated

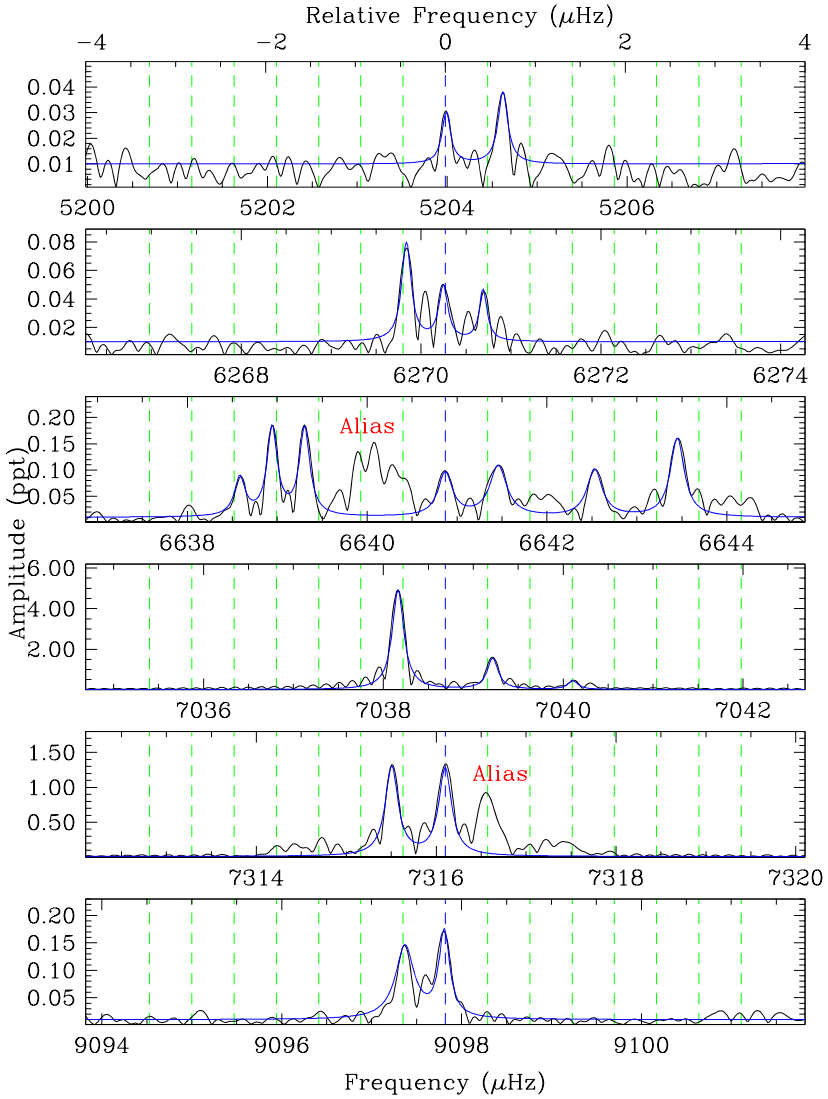


**Figure 4.** Samples of multiplets detected in UY Sex. Vertical (green in online version) lines indicate consecutive $\Delta m = 1$ spacings and solid (blue in online version) fitted lines indicate peaks considered intrinsic to each multiplet. The peaks marked 'Alias' are reflections across the Nyquist frequency.

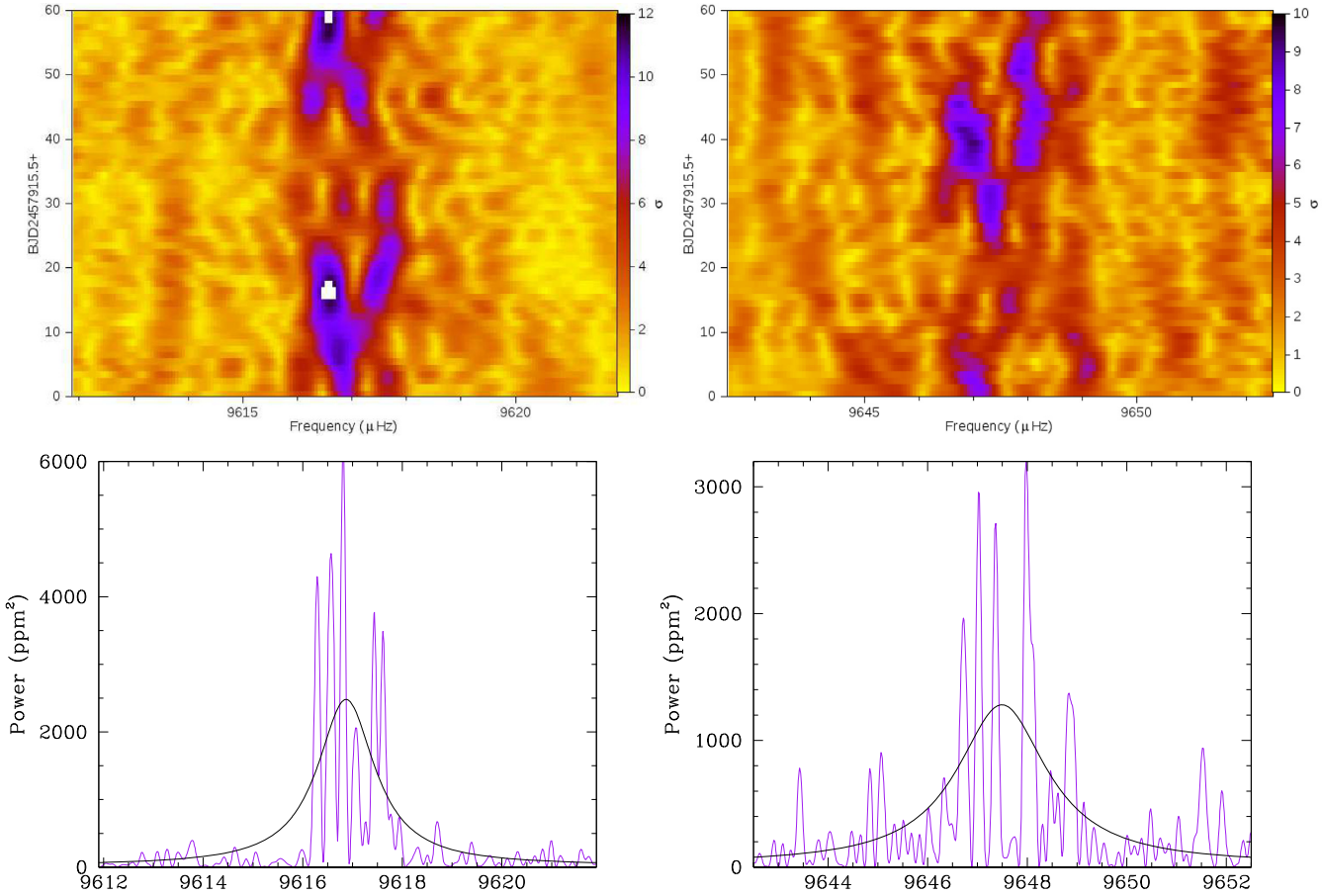


**Figure 5.** Fourier transforms showing two regions with stochastic pulsation properties for UY Sex. The top panels show the SFTs and the bottom panels show power spectra with the Lorentzian fit (black line).

**Table 2.** Lorentzian widths (LWs) and power ($H_i$) fitted to observations for UY Sex.

| Freq. (μHz) | LW (μHz) | $H_i$ (ppm$^2$) | Freq. (μHz) | LW (μHz) | $H_i$ (ppm$^2$) |
|---|---|---|---|---|---|
| 6824.3 | 1.8 | 8320 | 8663.5 | 1.2 | 620 |
| 6949.9 | 0.7 | 1590 | 9616.9 | 0.7 | 2460 |
| 7281.0 | 0.5 | 1360 | 9647.5 | 1.1 | 1260 |
| 7509.5 | 2.3 | 1720 | | | |

(thruster-corrected) light curves in ppt. A 2-d portion of the light curves is shown in Fig. 1. Our analyses then proceed with the use of Fourier transforms (FTs) and sliding FTs (SFTs), which time-slice the FTs to examine temporal evolution of the pulsations.

### 2.1 Pulsation analyses of UY Sex

UY Sex was observed by K2 during Campaign 14 between 2017 May 31 and August 19, a span of 80 d, which gives a 1.5/T resolution of 0.217 μHz. This results in 39 200 separate frequencies up to the Nyquist, which requires a detection threshold of 4.15$\sigma$ (0.029 ppt) (Bevington & Robinson 2003). We then visually determined which pulsations are above our detection threshold in the FT (Fig. 2) and note in the SFT if the amplitudes and frequencies are stable. The sliding SFTs used here span 20 d and are stepped by 1 d (shown in Figs 3 and 5). If they are stable, we fitted them using non-linear least-squares light-curve (NLLS) fitting and pre-whitening (e.g. Reed et al. 2004). If a pulsation frequency shows significant amplitude variation, traditional pre-whitening was ineffective and the pulsation was extracted using a Lorentzian fit where the Lorentzian widths are used as the frequency uncertainty. In a few cases, regions of power appeared stochastic in nature (e.g. Østensen et al. 2014; Reed et al. 2019) and those we also fitted with Lorentzians, but in those cases, we presume that the Lorentzian has a correlation with a physical attribute as in Østensen et al. (2014). Previous observations detected pulsation frequencies in K2's super-Nyquist region, so we used the tools described in Reed et al. (2018) to distinguish sub- from super-Nyquist. Table 1 provides the pulsation properties we consider intrinsic to UY Sex.

In total, we detected 97 periodicities we associate with pulsations. We detect all 19 pulsations detected in Kilkenny et al. (2002a), all five of those from Billères et al. (1997), and all nine of those from O'Donoghue et al. (1998). Charpinet et al. (2003) published some periods but only in a figure. We have compared those with our detections as best we could. All of the previous detections are noted in the sixth and twelfth columns of Table 1.

To associate pulsation frequencies with pulsation modes, we used frequency multiplets. Kilkenny et al. (2002a) reported multiplet frequency splittings of 1.05 μHz and so we began our search there. We do find those splittings, but we also find splittings at roughly half of that. Several of the detected multiplets are shown in Fig. 4. In total, we detected 18 multiplets including 44 frequency splittings. These average to 0.47 ± 0.08 μHz, which, assuming a Ledoux

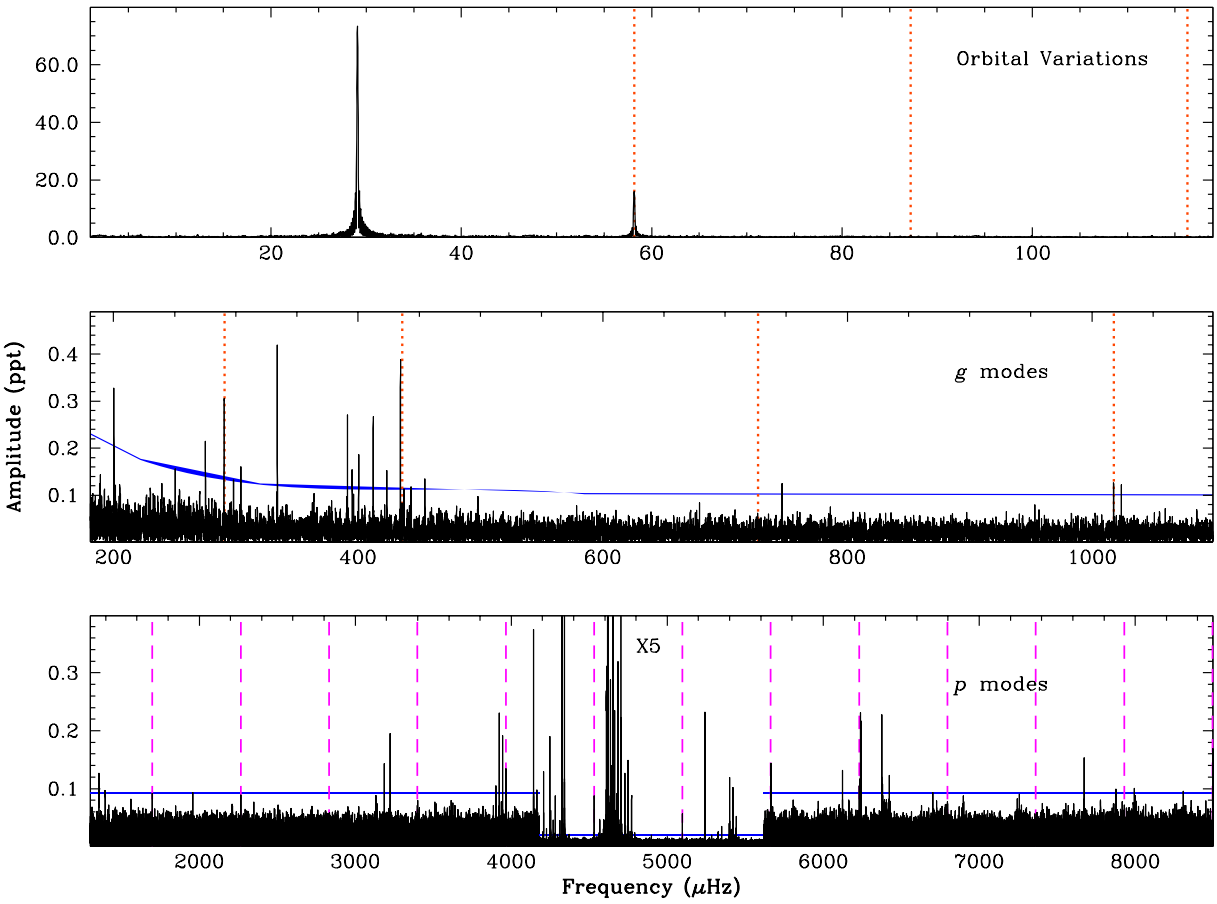


**Figure 6.** Fourier transform of V1405 Ori showing the different regions with variations. Dotted (red in online version) vertical lines indicate orbital overtones, dashed (magenta in online version) vertical lines indicate known data artefacts, and solid (blue in online version) horizontal lines indicate the 4.35$\sigma$ detection limit. Different regions are labelled and the middle of the p-mode region's amplitude is rescaled to show higher amplitude pulsations.

constant near zero, is a rotation period of 24.6 $\pm$ 3.5 d. As there are $2\ell + 1$ azimuthal modes, $\ell = 1$ modes make triplets, $\ell = 2$ modes make quintuplets, and so on. We used those to identify modes. Likewise, lower degree modes suffer less geometric cancellation (Pesnell 1985) and so should have higher amplitudes and therefore more complete multiplets. Lower-amplitude multiplets may have undetected members, and actually be higher degree than we interpret them to be. As such, the identifications provided in Table 1 may be considered lower limits on the degree, especially for low-amplitude multiplets.

As we have many multiplets, we can consider overtone spacings as well. p modes are not in an asymptotic regime, yet models have them spaced roughly 800–1 200 μHz apart. There are eight multiplets listed as $\ell = 1$ and the $m = 0$ components are separated by 922, 144, 1045, 1782, 484, 772, and 1028 μHz. If we presume that f12 and f13 are parts of an $\ell > 1$ multiplet, then the overtone spacings become 1066, 1045, 1782, 484, 772, and 1028 μHz. Except for the 484- μHz spacing, these all agree with model predictions and would correspond to $\Delta n = 1$, 1, 2, 1, and 1. The $\ell = 2$ overtone spacings are 1192, 699, and 671 μHz. These likely correspond to $\Delta n = 2$, 1, and 1. Of the five possible $\ell = 3$ multiplets, there are two separated by only 5 μHz, meaning that one of them is very likely $\ell > 3$. In that case, the overtones are separated by roughly 380 and 2580 μHz and the two $\ell = 4$ multiplets are separated by 492 μHz. These are small compared to models, but the higher degree mode identifications are less secure. As such, the best evidence suggests that overtone spacings are in rough agreement with model predictions.

Charpinet et al. (2003) published a model providing mode identifications for 16 periodicities. They list f31, f55, f89, and f91 as $\ell = 0$ and neither f31 nor f89 is part of multiplets, making those mode identifications likely. However, f55 and f95 are in multiplets, making them unlikely to be radial. Charpinet et al. (2003) list f38, f56, and f69 as $\ell = 1$ modes and we find agreement only for f69. f38 has too many multiplet members and we do not detect f56 in a multiplet at all, though its amplitude is low (S/N $<$ 25). They list f9, f41, and f59 as $\ell = 2$ modes. We find matches for f41 and f59 but not for f9, which is relatively high amplitude (S/N $>$ 50) and yet not part of a multiplet. They list f12 or f13, f47, f63, f76, and f91 as $\ell = 3$ and none of these directly match our findings. We detect only f12/f13 as a doublet though it does not fit well into the $\ell = 1$ overtone spacing, and so it could be $\ell > 1$. We find f47, f76, and f91 to be parts of $\ell = 4$, 2, and1 multiplets, respectively. We find their only $\ell = 4$ mode as part of an $\ell = 3$ multiplet. So of the 16 identified modes, five agree with our identifications, for seven we find multiplets contradicting their mode identifications, and our evidence is not especially constraining for the remainder.

UY Sex contains seven regions in the FT, which resemble stochastic oscillations as previously seen in three other sdBV stars (Østensen et al. 2014; Reed et al. 2019). Some examples of these are shown in Fig. 5 with their properties provided in Table 2. Similar

**Table 3.** High-frequency periodicities in V1405 Ori.

| ID | Freq. (μHz) | Amp. (ppt) | S/N | $\ell$, $m$ | $f_{2004/5}$ |
|---|---|---|---|---|---|
| f1 | 1356.497 (16) | 0.123 (24) | 6.08 | 1, −1 | |
| f2 | 1396.754 (22) | 0.090 (24) | 4.68 | 1, 1 | |
| f3 | 3185.445 (14) | 0.141 (24) | 6.71 | 1, −1 | |
| f4 | 3223.754 (10) | 0.193 (24) | 9.19 | 1, 1 | |
| f5 | 3901.256 (20) | 0.103 (25) | 4.90 | 2, −2 | |
| f6 | 3923.274 (9) | 0.228 (25) | 10.86 | 2, −1 | |
| f7 | 3945.278 (10) | 0.200 (25) | 9.52 | 2, 0 | |
| f8 | 3965.328 (14) | 0.146 (25) | 6.95 | 2, 1 | |
| f9 | 4142.443 (8) | 0.373 (37) | 17.76 | | b + 1*d* |
| f10 | 4163.617 (30) | 0.100 (37) | 4.76 | | |
| f11 | 4205.785 (5) | 0.609 (37) | 29.00 | 2, −2 | b |
| f12 | 4206.002 (18) | 0.178 (37) | 8.48 | | |
| f13 | 4226.773 (20) | 0.148 (37) | 7.05 | 2, −1 | |
| f14 | 4247.840 (3) | 0.915 (37) | 43.57 | 2, 0 | b + 1*d* |
| f15 | 4253.732 (10) | 0.309 (37) | 14.71 | | |
| f16 | 4268.797 (14) | 0.212 (37) | 10.10 | 2, 1 | |
| f17 | 4273.757 (26) | 0.114 (37) | 5.43 | | |
| f18 | 4282.811 (7) | 0.423 (37) | 20.14 | 1, −1 | |
| f19 | 4307.686 (29) | 0.105 (37) | 5.00 | | |
| f20 | 4311.896 (13) | 0.238 (37) | 11.332 | | a |
| f21 | 4324.383 (1) | 2.344 (37) | 111.62 | 1, 0 | a, b |
| f22 | 4340.969 (1) | 2.857 (37) | 136.05 | | b |
| f23 | 4567.462 (10) | 0.197 (25) | 9.38 | | |
| f24 | 4577.049 (19) | 0.109 (25) | 5.19 | 1, 0 | |
| f25 | 4587.253 (18) | 0.110 (25) | 5.24 | 1, 1 | b |
| f26[1] | 4589.070 (80) | 0.110 | 5.24 | 1, 1 | |
| f27 | 4592.178 (9) | 0.217 (25) | 10.33 | | |
| f28 | 4599.553 (9) | 0.233 (25) | 11.10 | | |
| f29[1] | 4604.040 (80) | 0.110 | 5.24 | | b |
| f30[1] | 4610.392 (180) | 1.370 | 65.24 | | a |
| f31[1] | 4612.350 (110) | 0.310 | 14.76 | | |
| f32 | 4615.969 (6) | 0.494 (35) | 23.52 | | |
| f33 | 4616.298 (6) | 0.513 (35) | 24.430 | | |
| f34 | 4618.154 (1) | 4.450 (35) | 211.90 | | |
| f35 | 4621.265 (1) | 3.159 (35) | 150.43 | 4, −4 | b |
| f36 | 4624.077 (7) | 0.397 (35) | 18.90 | | |
| f37[1] | 4625.020 (90) | 0.160 | 7.62 | | |
| f38 | 4625.606 (9) | 0.302 (35) | 14.38 | | |
| f39[1] | 4625.910 (100) | 0.210 | 10.00 | | |
| f40[1] | 4632.360 (150) | 0.290 | 13.8 | | |
| f41[1] | 4634.180 (80) | 0.120 | 5.71 | | a |
| f42 | 4635.199 (2) | 1.359 (27) | 64.71 | | |
| f43[1] | 4639.450 (150) | 0.180 | 8.57 | | |
| f44[1] | 4640.560 (380) | 0.600 | 28.57 | 4, −3 | |
| f45[1] | 4643.000 (100) | 0.300 | 14.29 | | |
| f46 | 4643.500 (3) | 0.624 (27) | 29.71 | | |
| f47 | 4645.373 (5) | 0.405 (27) | 19.29 | | |
| f48[1] | 4646.370 (100) | 0.130 | 6.19 | | |
| f49 | 4647.234 (7) | 0.293 (27) | 13.95 | | |
| f50[1] | 4650.330 (130) | 0.220 | 10.48 | | |
| f51 | 4653.155 (1) | 2.108 (27) | 100.38 | | |
| f52 | 4654.998 (2) | 1.358 (27) | 64.67 | | |
| f53 | 4655.227 (2) | 1.077 (27) | 51.29 | | |
| f54 | 4662.183 (2) | 1.082 (27) | 51.52 | 4, −2 | |
| f55[1] | 4664.000 (110) | 0.120 | 5.71 | | b |
| f56[1] | 4667.590 (110) | 0.090 | 4.29 | | |
| f57[1] | 4668.580 (190) | 0.270 | 12.86 | | |
| f58 | 4674.468 (9) | 0.256 (27) | 12.19 | | b |
| f59 | 4674.934 (16) | 0.145 (27) | 6.90 | | |
| f60 | 4676.319 (5) | 0.440 (27) | 20.95 | | |
| f61 | 4679.447 (19) | 0.116 (27) | 5.52 | | a |
| f62 | 4683.163 (1) | 1.514 (27) | 72.10 | 4, −1 | |
| f63 | 4685.828 (14) | 0.164 (27) | 7.81 | | |
| f64 | 4686.339 (10) | 0.234 (27) | 11.14 | | |
| f65 | 4688.633 (13) | 0.170 (27) | 8.10 | | |
| f66 | 4691.294 (14) | 0.156 (27) | 7.43 | | |
| f67 | 4703.412 (6) | 0.702 (38) | 33.43 | | b |
| f68 | 4703.538 (1) | 4.534 (38) | 215.90 | 4, 0 | |
| f69[1] | 4707.300 (100) | 0.130 | 6.19 | | a |
| f70 | 4728.253 (4) | 0.528 (27) | 25.14 | 4, 1 | |
| f71[1] | 4730.100 (100) | 0.140 | 6.67 | | |
| f72[1] | 4732.590 (190) | 0.110 | 5.24 | | |
| f73[1] | 4734.460 (11) | 0.095 | 4.52 | | |
| f74 | 4749.443 (3) | 0.705 (25) | 33.57 | 4, 2 | b |
| f75 | 4749.619 (7) | 0.320 (25) | 15.24 | | |
| f76 | 4750.688 (20) | 0.101 (24) | 4.81 | | |
| f77 | 4771.204 (5) | 0.421 (27) | 20.05 | 4, 3 | |
| f78 | 5242.247 (2) | 1.104 (25) | 52.57 | | |
| f79 | 5284.769 (20) | 0.103 (25) | 4.90 | | |
| f80 | 5326.496 (17) | 0.121 (25) | 5.76 | | |
| f81 | 5327.534 (20) | 0.099 (25) | 4.71 | | |
| f82 | 5347.924 (13) | 0.159 (25) | 7.57 | | b + 1*d* |
| f83 | 5397.647 (11) | 0.192 (25) | 9.14 | | |
| f84 | 5399.503 (11) | 0.193 (25) | 9.19 | 1, −1 | |
| f85 | 5399.831 (4) | 0.578 (25) | 27.52 | | |
| f86[1] | 5410.630 (210) | 0.140 | 6.67 | | |
| f87 | 5419.335 (14) | 0.144 (25) | 6.86 | | b |
| f88 | 5420.152 (4) | 0.486 (25) | 23.14 | 1, 0 | |
| f89 | 5420.460 (11) | 0.189 (25) | 9.00 | | |
| f90 | 5421.190 (10) | 0.196 (25) | 9.33 | a | |
| f91[1] | 5428.900 (110) | 0.085 | 4.05 | | |
| f92[1] | 5440.320 (260) | 0.145 | 6.90 | 1, 1 | |
| f93 | 5441.724 (8) | 0.247 (25) | 11.76 | | b |
| f94 | 6123.846 (17) | 0.119 (24) | 5.67 | | |
| f95 | 6162.997 (20) | 0.097 (24) | 4.62 | | |
| f96[1] | 6231.230 (110) | 0.095 | 4.52 | | |
| f97 | 6236.004 (16) | 0.127 (25) | 6.05 | | b |
| f98 | 6236.294 (17) | 0.119 (25) | 5.67 | | |
| f99[1] | 6236.860 (200) | 0.115 | 5.48 | | |
| f100[1] | 6239.640 (150) | 0.230 | 10.95 | | |
| f101 | 6240.999 (8) | 0.241 (24) | 11.48 | | b |
| f102 | 6375.865 (9) | 0.231 (24) | 11.00 | | |
| f103 | 6376.803 (17) | 0.114 (24) | 5.43 | | |
| f104 | 6379.533 (18) | 0.108 (24) | 5.14 | | b |
| f105 | 7672.630 (12) | 0.168 (24) | 8.00 | | |
| f106[1] | 7875.360 (110) | 0.100 | 4.76 | | |
| f107 | 8308.282 (19) | 0.103 (24) | 4.90 | | |

**Table 3** – *continued*

Notes. [1]These frequencies are fitted with Lorentzians as NLLS fitting would not converge to a solution. a = Koen et al. (1999), b = Reed et al. (2010).

to the two stars in Reed et al. (2019), the majority of pulsations in UY Sex *do not* show stochastic properties. Though not mentioned in those papers, so-called 'messy' regions in Balloon 090100001 (Baran, Pigulski & O'Toole 2008) and KIC 3527751 (Foster et al. 2015) may also have stochastic properties, indicating that there may be more examples yet to be identified. The current lack of an adequate source for generating them, particularly when outnumbered by apparently stable oscillations, makes stochastic oscillations worth a mention in this paper.

### 2.2 Variation analyses of V1405 Ori

V1405 Ori was observed by K2 during Campaign 13 between 2017 March 8 and May 27, a span of nearly 81 d, which has a

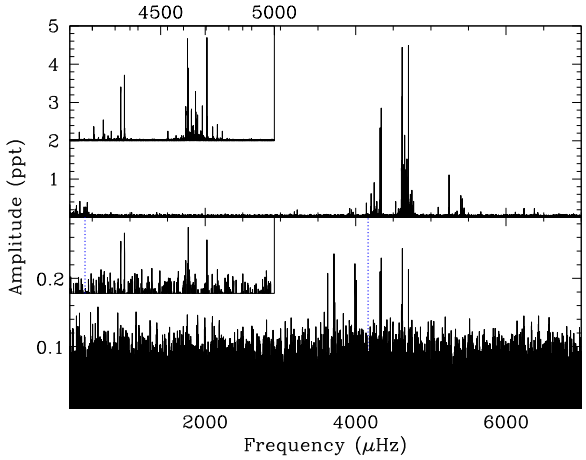


**Figure 7.** Comparison of the FT from K2 data (top) and that from *TESS* (bottom) for V1405 Ori. The dashed blue line in the *TESS* FT indicates the *TESS* Nyquist frequency. Insets show just the 4100–5000 μHz regions.

1.5/$T$ resolution of 0.215 μHz. We used a 4.35$\sigma$ detection limit (Bevington & Robinson 2003) of 0.093 ppt in the p-mode region, with a higher limit in the g-mode region, as $\sigma$ is higher there. The FT for V1405 Ori is shown in Fig. 6, including lines for the detection limit, orbital overtones, and known space craft artefacts. Our FT also provides a very accurate period for the binary of 0.398023 ± 0.000003.

The FT is dominated by frequencies between 4000 and 5500μHz, which we attribute to p-mode pulsations. All of the pulsations are below the Nyquist frequency, and so no sub/super-Nyquist distinction tests (Reed et al. 2018) were required. Unusual for K2-duration observations of sdBV stars, most of the pulsations were sufficiently stable for NLLS analysis. We were able to fit and pre-whiten 78 frequencies between 3100 and 8310μHz. Twenty-seven additional peaks, for which pre-whitening failed to remove the peak, were Lorentzian fitted to the FT. We use the Lorentzian width as an error on the frequency, but do not report amplitude errors, as amplitude variability is the leading cause of pre-whitening failure. Pulsations are listed in Table 3.

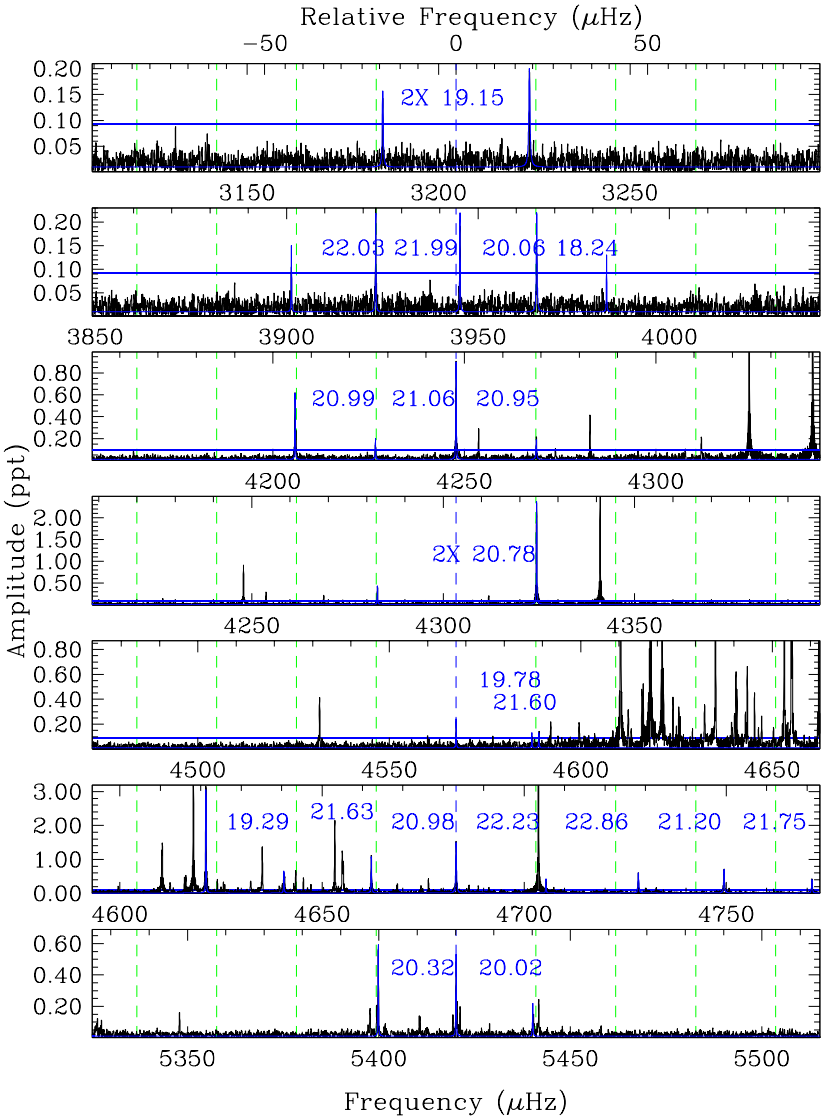


**Figure 8.** Multiplets detected in V1405 Ori. Frequencies attributed to each multiplet are fitted with green lines and separations are listed.

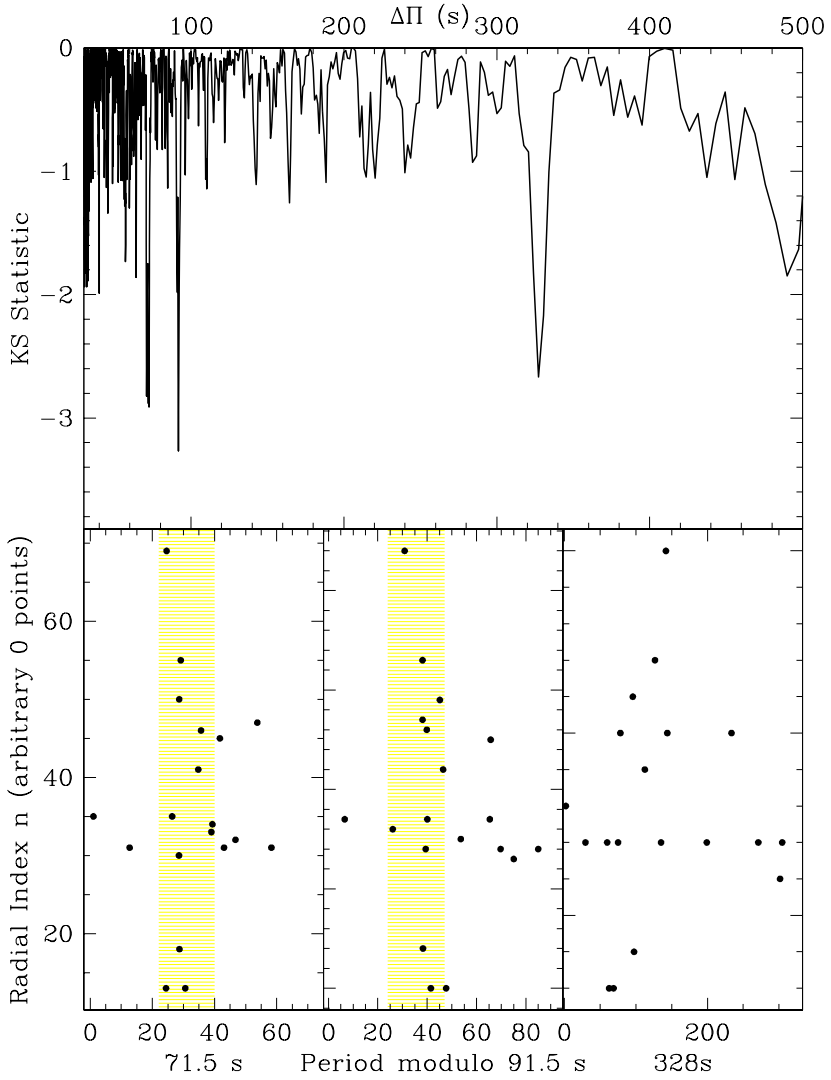


**Figure 9.** KS test (top panel) for V1405 Ori and Echelle diagrams for the three deepest troughs. Periods that fit a sequence should line up vertically, indicated by the shaded regions for the most likely sequences, which are also included in Table 4.

V1405 Ori was also observed by *TESS* (the *Transiting Exoplanet Survey Satellite*[1]) in sector 5 (2018 November 15 to December 11). We downloaded the *TESS* light curve, sigma-clipped at $5\sigma$, removed long-term trends (>3 d), and made an FT. Fig. 7 compares the FTs from K2 and *TESS*. V1405 Ori is near the faint-end of *TESS*'s range, and with pixels over five times larger than Kepler's, contamination from neighbouring stars is severe, reducing the pulsation amplitudes. However, the four highest amplitude periodicities do appear in the *TESS* FT, though at *TESS*'s 2 m sampling, they are all super-Nyquist. The only result that can be inferred by comparing the K2 and *TESS* FTs is that relative amplitudes changed between the two data sets (roughly 1.5 yr), although with *TESS*'s poorer frequency resolution, even this could be caused by unresolved periodicities.

We recovered all the frequencies listed in Koen et al. (1999) and Reed et al. (2010), though some are at daily aliases away from the original periodicity. These are labelled in columns 6 and 12 of Table 3.

[1]https://tess.mit.edu

The binary frequency is 29.07889 ± 0.00024 μHz, and as the Ledoux constant for p modes is near zero (Charpinet et al. 2000), if tidally locked, azimuthal components would be split by that amount. From spectroscopic velocities, the orbital inclination must be close to 90°, though no eclipses are observed, so we expect that the inclination is good for observing azimuthal components. Frequency multiplets can then be used to identify pulsation modes, which has been a very useful tool for sdBV stars (e.g. Baran et al. 2012). An inspection of the frequencies did not reveal any splittings near 29 μHz but rather a value near 21 μHz. A total of eight possible multiplets, most shown in Fig. 8, involving 19 splittings average to a frequency splitting of 20.85 ± 1.16 μHz. This would correspond to a rotation period of 0.555 ± 0.029 d. This would be only slightly subsynchronous to the binary period. The azimuthal components were used to determine the degree and the minimum values are provided in Table 3.

We can examine the overtone spacings of the p-mode multiplets. For $\ell = 1$, this is 1828, 1120, 253, and 843 μHz and for $\ell = 2$, it is 303 μHz. The two smaller spacings are similar in size to those found in Baran et al. (2012), but as some of the components have quite low amplitudes, it is possible that they have degrees higher than we

**Table 4.** Low-frequency period list for V1405 Ori.

| ID | Freq. μHz | Per. Days | Amp. ppt | | | |
|---|---|---|---|---|---|---|
| O0 | 29.07889 (24) | 0.3980232 (33) d | 74.6 | | | |
| O1[a] | 58.1629 | | 15.9 | | | |
| ID | Freq μHz | Per Sec | Amp ppt | S/N | $n$ ($\ell = 3/4$) | $\frac{\Delta P}{P}$ % |
| fA | 200.326 (6) | 4991.88 (14) | 0.316 (22) | 7.18 | 54/69 | −6.9/−8.2 |
| fB | 250.462 (12) | 3992.62 (18) | 0.158 (22) | 4.24 | 43/55 | −1.0/−2.1 |
| fC | 275.207 (8) | 3633.62 (11) | 0.222 (22) | 5.85 | 39/50 | 6.0/−2.8 |
| fD[b(10)] | 290.391 (6) | 3443.63 (7) | 0.312 (22) | 8.35 | 37/– | −2.1/– |
| fE | 298.166 (13) | 3353.84 (15) | 0.138 (22) | 4.22 | 36/46 | −0.4/6.9 |
| fF | 304.117 (11) | 3288.21 (12) | 0.160 (22) | 5.35 | – | – |
| fG | 333.951 (4) | 2994.45 (4) | 0.421 (22) | 14.85 | 32/41 | 6.1/5.6 |
| fH | 391.259 (7) | 2555.85 (4) | 0.270 (22) | 9.95 | –/35 | –/−6.2 |
| fI | 395.172 (12) | 2530.54 (7) | 0.156 (22) | 5.53i | 27/– | −1.8/– |
| fJ | 400.466 (10) | 2497.09 (6) | 0.190 (22) | 7.06 | –/34 | –/11.8 |
| fK | 412.361 (7) | 2425.06 (4) | 0.271 (22) | 10.04 | –/33 | –/11.3 |
| fL | 423.530 (13) | 2361.11 (8) | 0.135 (22) | 5.93 | 25/– | 12.7/– |
| fM | 434.600 (5) | 2300.96 (3) | 0.383 (22) | 15.42 | – | – |
| fN[b(15)] | 437.497 (15) | 2285.73 (8) | 0.119 (22) | 4.35 | – | – |
| fO | 443.382 (14) | 2255.39 (7) | 0.125 (22) | 4.75 | 24/– | −3.1/– |
| fP | 454.639 (14) | 2199.55 (7) | 0.126 (22) | 5.66 | –/30 | –/−3.2 |
| fQ | 746.657 (14) | 1339.30 (2) | 0.146 (24) | 5.22 | 14/18 | −6.2/−3.2 |
| fR[b(35)] | 1017.635 (16) | 982.67 (2) | 0.123 (24) | 6.08 | –/13 | –/−0.6 |
| fS | 1024.077 (15) | 976.49 (1) | 0.129 (24) | 5.61 | 10/13 | −3.4/−9.3 |

*Notes.* [a]These measurement are by eye.
[b]These frequencies are within 1% of an orbital overtone, given within parentheses.

have assigned. As such, it seems fairly likely that V1405 Ori has p-mode overtone spacings in agreement with model predictions.

We detect 21 periodicities in the low-frequency region, most of which we associate with g-mode pulsations. Two frequencies $> 1000$ μHz are included in this set because of the large gap to higher frequencies. While these may be mixed-mode pulsations, they fit the asymptotic sequence discussed below, which means that they are most likely g-mode pulsations.

Typical to g modes in sdBV stars are asymptotic period sequences with spacings near 250 s for $\ell = 1$ (Reed et al. 2011). We use the Kolmogorov–Smirnov (KS) test to search for commonly occurring spacings. The result of this test is shown in the top panel of Fig. 9. The KS test indicates spacings near 71, 91, and 328 s but none near 250 s. We produced Echelle diagrams for each of these splittings, making adjustments by eye to achieve the best fit (shown in Fig. 9). The periods indicated by the diagrams were then least-squares fitted. Both of the shorter sequences included observed periods matching 11 overtones, with least-squares fitting of 71.70 ± 0.10 and 91.32 ± 0.14 s, respectively. The longer, 328- s sequence fitted only six periods, and so we presume that this is not an asymptotic sequence. The 71 and 91- s sequences could be $\ell = 3$ and 4, if the $\ell = 1$ spacing is near 225 s or $\ell = 4$ and 5, if the $\ell = 1$ spacing is near 285 s. We favour the former, as hotter sdBV stars tend to shorter overtone spacings (Baran et al. 2012; Reed et al. 2019) and it fits both sequences more closely. Identifications for that scheme are provided in Table 4.

Table 4 lists the orbital frequency, as well as the first three overtones with their amplitudes and shown in Fig. 6 as dotted vertical lines for overtones that appear near peaks in the FT. Orbital overtones are caused by non-sinusoidal features in the light curve. While no features are detected above the noise limit for O4 and above, there are three frequencies (fD, fN, and fR) that are very close to orbital overtones. fD, fN, and fR deviate from precise overtones only by 0.4, 0.3, and 0.4 per cent, respectively, and fD and fR fit asymptotic relations while fN does not. These will be discussed further in Section 4.2.

As we know both the binary period and the splitting of p-mode frequency multiplets, we should be able to find g-mode frequency multiplets commensurate with either of those. For $\ell = 3$, 4, and 5, the Ledoux constant, derived from asymptotic relations (Ledoux 1951), is small ($C_{n,\ell} = 0.08$, 0.05, and 0.03, respectively) and we searched for splittings around 20 and 29 μHz. The splittings between fA, fB, and fC are $2 \times 25$ and 25 μHz and multiples of that splitting are shown in the top panel of Fig. 10. However, the period difference at those wavelengths are 1000 and 360 s, and all three are associated with asymptotic period sequences. fJ through fM make an uneven multiplet with spacings of 11.9, 11.2, and 11.1 μHz, respectively, which would need to be $\ell \geq 2$. The Ledoux constant for $\ell = 2$ is $C_{n,\ell} = 0.17$, these do not fit either of the expected splittings (regardless of degree), and again, all save one of these frequencies are associated with asymptotic sequences. In searching the frequencies that are not associated with asymptotic sequences, we see a couple of splittings near 3 and 6 μHz. These are shown in the bottom three panels of Fig. 10. If these are intrinsic frequency splittings indicative of rotation, then their average value of 2.87 ± 0.15 μHz would mean a rotation period of 4.40 ± 0.22 for $\ell = 3$ and 4.16 ± 0.21 for $\ell = 5$. Either of these would mean a core with a longer rotation period than the envelope, similar to previous detections (Foster et al. 2015; Baran et al. 2017; Reed et al. 2019).

The g modes of V1405 Ori present a complex picture when applying the usual tools of asymptotic period sequences and frequency multiplets with no clearly distinct mode identifications. We provide our *best estimate* mode identifications in Table 4 but with a significant warning that the mode identifications are not very secure.

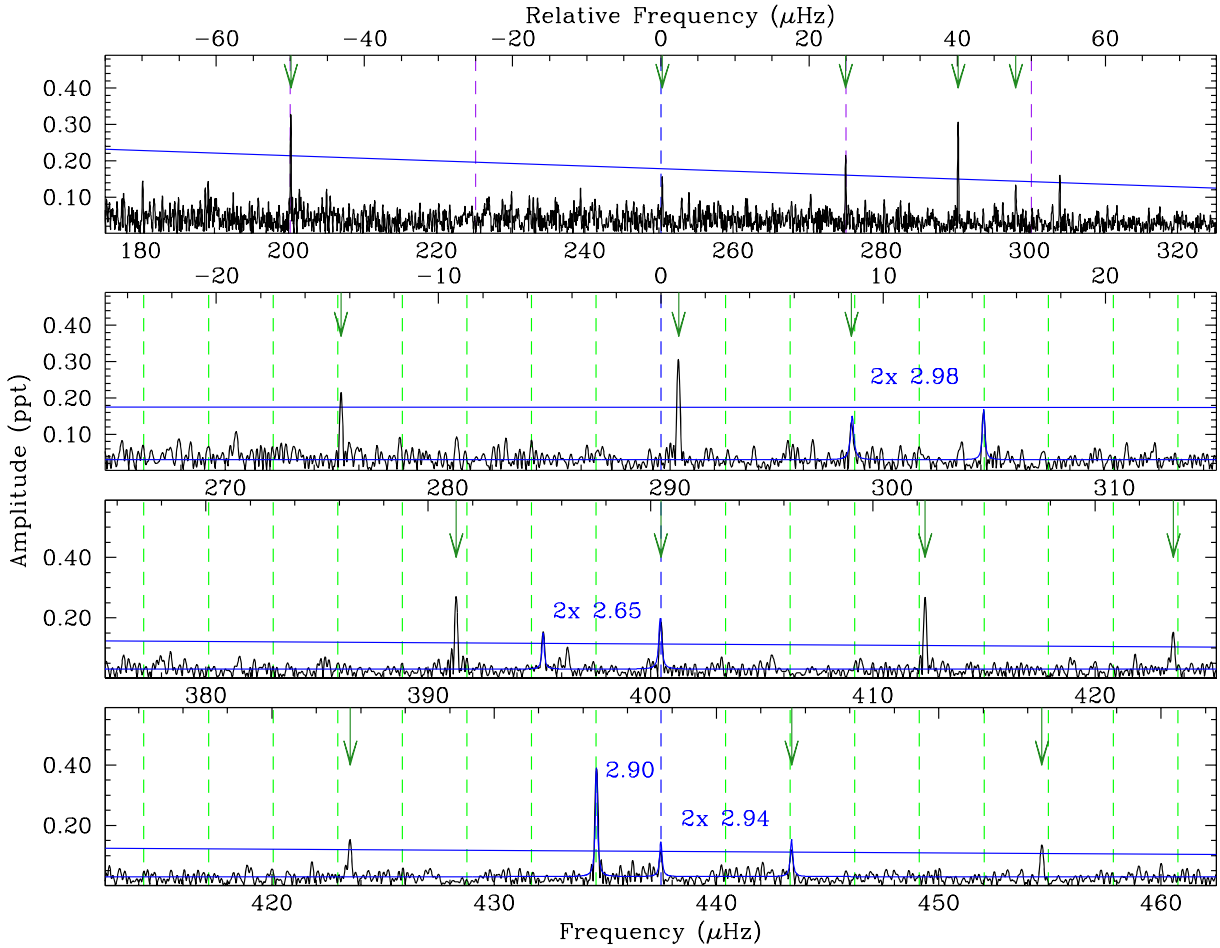


**Figure 10.** Possible frequency multiplets in the low-frequency region of V1405 Ori. Dotted vertical lines indicate frequency splittings of 25 μHz in the top panel and 2.91 μHz in the other panels. Possible splittings are labelled by the difference in μHz. Solid blue line is the detection limit and green arrows indicate frequencies that also fit into asymptotic period sequences.

## 3 SPECTROSCOPIC OBSERVATIONS

As part of our follow-up spectroscopic survey (Telting et al. 2012) of Kepler-observed sdBV stars, we used ALFOSC at the 2.6 m Nordic Optical Telescope (see Djupvik & Andersen 2010, for a description of instrumentation), with grism #18 and a 0.5 arcsec slit providing $R = 2000$ resolution or 2.2 Å to obtain eight spectra of UY Sex and three of V1405 Ori. The exposure times were 300 s or 400 s for UY Sex, giving $64 < S/N < 130$, and were 400 s for V1405 Ori, yielding $39 < S/N < 51$.

The data were homogeneously reduced and analysed as described in Telting et al. (2012), Reed et al. (2016), using IRAF for bias subtraction, removal of pixel-to-pixel sensitivity variations, optimal spectral extraction, and wavelength calibration based on arc-lamp spectra. The target spectra and the mid-exposure times were shifted to the barycentric frame of the Solar system. For V1405 Ori, individual spectra were corrected to the system velocity before co-adding to remove possible orbital motion. The average spectra have $S/N = 310$ for UY Sex, and $S/N = 70$ for V1405 Ori.

We determined $T_{\rm eff}$ and $\log g$ from the mean spectra using the H/He LTE grid of Heber, Reid & Werner (1999) for consistency with the *Kepler* main field survey of Østensen et al. (2010), Østensen et al. (2011). We used all the Balmer lines from H$\beta$ to H14 and the four strongest He I lines for the fit. The errors listed on the measurements are the formal errors of the fit, which reflect the S/N of the mean spectrum. These values and errors are relative to the LTE model grid and do not reflect any systematic effects caused by the assumptions underlying those models. Such systematic effects depend strongly on the details of the model grid such as the assumed metal content and can be as large as 2.5 kK in effective temperature and 0.2 in $\log g/{\rm cm\,s^{-2}}$.

As V1405 Ori is in a short, likely near-synchronized orbit, and as p-mode splittings (see Section 3.2) indicate a rotation period near 0.55 d, we investigated if rotational broadening has any effect on the measured atmospheric parameters. For a typical radius of $R/{\rm R}_\odot = 0.2$, and assuming $P = 0.55$ d, we derive that the rotational broadening should be on the order of $V \sin i = 18\,{\rm km\,s^{-1}}$ for high orbital inclination. Given the quality and resolution of the ALFOSC average spectrum, we find no significant change when using a $V \sin i$ with no rotational broadening.

### 3.1 Spectral energy distribution

The spectral energy distribution (SED) can be used to derive an independent set of spectral parameters and when coupled with parallax, can provide luminosity ($L$), radii ($R$), and masses ($M$). Our photometric SED is fitted with TMAP (Tübingen NLTE Model-Atmosphere Package, Werner et al. 2003) atmosphere models for the sdB components and Kurucz atmosphere models (Kurucz 1979)

**Table 5.** Photometric values used in our SED fits. Magnitudes are from APASS (Henden et al. 2015), 2MASS (Skrutskie et al. 2006), WISE (Cutri & et al. 2012), and *Gaia* (Gaia Collaboration et al. 2016, 2018; Riello et al. 2018; Evans et al. 2018) with errors within parentheses.

| Band | UY Sex | V1405 Ori |
|---|---|---|
| JOHNSON.U | | 14.510 (50) |
| JOHNSON.B | | 15.260 (50) |
| JOHNSON.V | | 15.080 (50) |
| APASS.B | 13.222 (43) | 15.297 (19) |
| APASS.V | 13.468 (8) | 15.120 (90) |
| APASS.G | 13.239 (11) | 15.140 (32) |
| APASS.R | 13.700 (21) | 15.044 (102) |
| APASS.I | 14.067 (5) | 15.240 (184) |
| GAIA2.G | 13.433 (1) | 14.970 (27) |
| GAIA2.BP | 13.212 (7) | 15.062 (77) |
| GAIA2.RP | 13.730 (3) | 14.715 (135) |
| 2MASS.J | 14.152 (29) | 14.574 (31) |
| 2MASS.H | 14.214 (47) | 14.677 (46) |
| 2MASS.$K_S$ | 14.319 (75) | 14.458 (79) |
| WISE.W1 | 14.418 (32) | 14.375 (34) |
| WISE.W2 | 14.602 (65) | 14.335 (65) |

for main sequence (MS) components. The EMCEE MCMC sampler (Foreman-Mackey et al. 2013) was used to fit between observed SEDs and models and provides the errors on the parameters. A detailed description of the SED fitting process is given in Vos et al. (2013) and Vos et al. (2017). Magnitudes from photometric sources are provided in Table 5 and reddening was obtained from the dust maps of Lallement et al. (2019). In the SED fitting process, $T_{\rm eff}$ and $\log g$ of the sdB star are kept fixed at the spectroscopically determined parameters and errors on the spectroscopic parameters are included in the fits.

**Table 6.** Spectroscopic and SED/parallax results for UY Sex. The *Gaia* distance is from Bailer-Jones et al. (2018).

| Parameter | Value | Source |
|---|---|---|
| $^a T_{\rm eff}$ (kK) | $33.03 \pm 0.22$ | NOT spectra |
| $^a \log g/{\rm cm\,s^{-2}}$ | $5.867 \pm 0.006$ | NOT spectra |
| $\log n_{\rm He}/n_{\rm H}$ | $-1.957 \pm 0.015$ | NOT spectra |
| $E(B-V)$ | 0.01 | Lallement et al. (2019) |
| $T_{\rm eff}$ (kK) | $33.09 \pm 0.20$ | SED |
| $L/{\rm L}_\odot$ | $25.86^{+3.28}_{-2.61}$ | SED |
| $R/{\rm R}_\odot$ | $0.17 \pm 0.01$ | SED |
| $d$ (pc) | $693^{+43}_{-36}$ | SED |
| $d$ (pc) | $674^{+39}_{-35}$ | GAIA |

*Note.* [a]Only fitting errors are provided. Differences between atmospheric methods and fitting methods can result in systematic changes up to 2 kK in $T_{\rm eff}$ and 0.2 in $\log g/{\rm cm\,s^{-2}}$.

### 3.2 UY Sex

As UY Sex is an apparently single sdB star, for which we have spectra, *Gaia* parallax, and several sources for photometry, it should be possible to determine its radius, luminosity, and mass. The SED results are shown in Fig. 11 and listed in Table 6, except for mass, which is discussed in Section 4.3. The SED parameters are reasonable.

### 3.3 V1405 Ori

We folded the K2 observations over the binary period and these are shown in Fig. 12. The appearance is typical for an sdB star with an M-dwarf companion in a so-called 'reflection-effect' binary. The appearance of the folded K2 light curve and a lack of companion lines in our spectra mean that we have an a priori expectation for

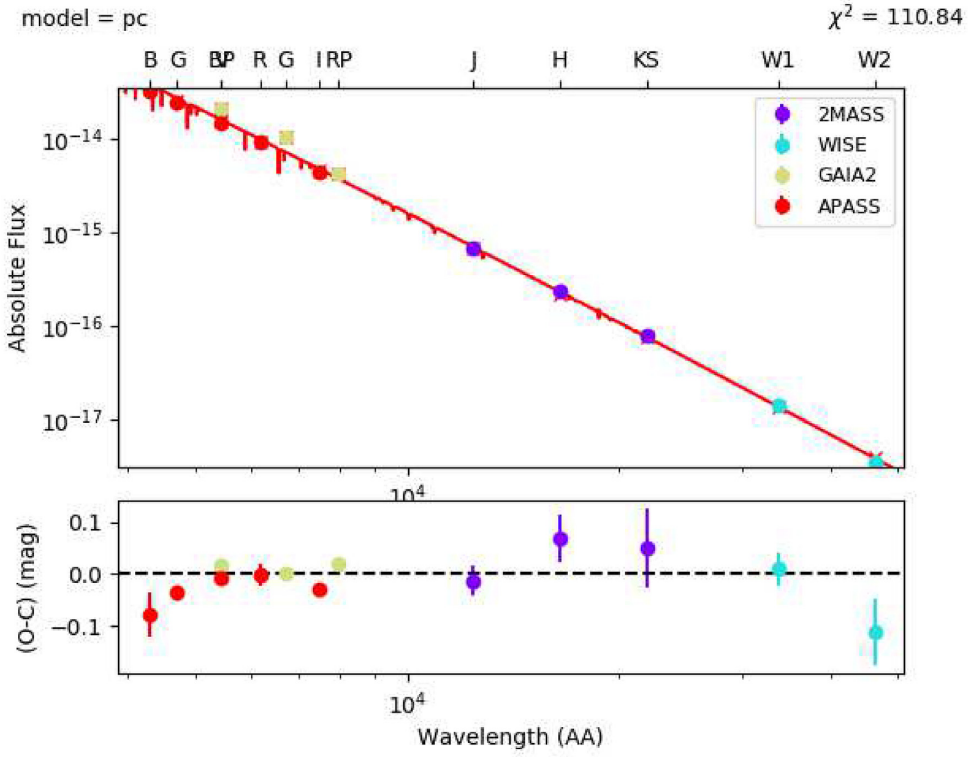


**Figure 11.** Spectral energy distribution for UY Sex.

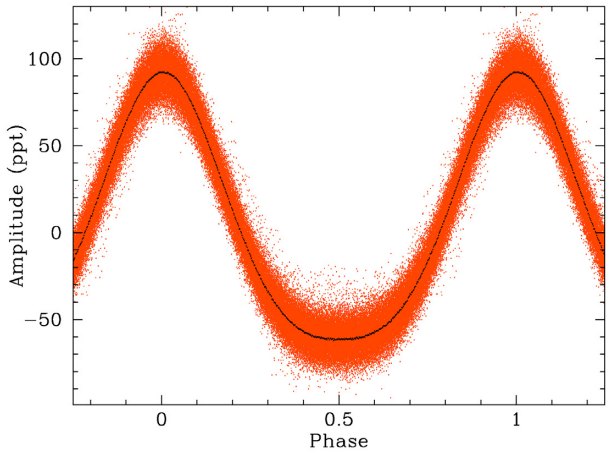


**Figure 12.** Light curve of K2 data for V1405 Ori folded over the binary period (red points) and binned (black points). Slightly more than one phase is shown for clarity.

**Table 7.** Spectroscopic and SED/parallax results for V1405 Ori. The *Gaia* distance is from Bailer-Jones et al. (2018).

| Parameter | Value | Source |
|---|---|---|
| $d$ (pc) | $715^{+22}_{-17}$ | SED |
| $d$ (pc) | 699 ± 19 | GAIA |
| $E(B-V)$ | 0.25 ± 0.05 | Lallement et al. (2019) |
| | sdB | |
| $T_{\rm eff}$ (kK)[a] | 31.36 ± 0.24 | NOT spectrum |
| $\log g/{\rm cm\,s^{-2}}$[a] | 5.573 ± 0.044 | NOT spectrum |
| $\log n_{\rm He}/n_{\rm H}$ | −2.6462 ± 0.1017 | NOT spectrum |
| $T_{\rm eff}$ (kK)[a] | $25.4^{+7.0}_{-3.0}$ | SED[b] |
| $R/{\rm R}_\odot$ | 0.11 ± 0.03 | SED[b] |
| $R/{\rm R}_\odot$ | 0.08 ± 0.01 | SED[c] |
| | MS companion | |
| $T_{\rm eff}$ (kK)[a] | 8.02 ± 0.20 | SED[b] |
| $R/{\rm R}_\odot$ | 0.31 ± 0.02 | SED[b] |
| $T_{\rm eff}$ (kK)[a] | 8.17 ± 0.12 | SED[c] |
| $R/{\rm R}_\odot$ | 0.33 ± 0.02 | SED[c] |

*Notes.* [a]Only fitting errors are provided. Differences between atmospheric models and fitting models can result in systematic changes up to 2 kK in $T_{\rm eff}$ and 0.2 in $\log g/{\rm cm\,s^{-2}}$.
[b]SED results where $T_{\rm eff}$ was free to vary.
[c]SED results where $T_{\rm eff}$ was fixed to the spectroscopic value of 31.30 ± 0.25 kK.

our SED fitting. The photometric measurements listed in Table 5 are products of multiple observations, and so we presume that they represent values averaged over the orbit. Reddening is quite high in the direction of V1405 Ori, which likely presents a problem.

For V1405 Ori, we also allowed $T_{\rm eff}$ of the sdB to vary and the parameters of the companion and the radius of the sdB are free and allowed to vary. The SED results are provided in Table 7 and shown in Fig. 13. $T_{\rm eff}$ for the companion is a little higher than that measured for the sdB + dM binary EQ Psc (Baran et al. 2019), which is consistent with a closer orbit of a hotter sdB star. The derived parameters for the cool companion seem fairly robust in that even when the reddening is allowed to vary freely, the effective temperature derived for the companion does not vary by more than 500 K. Likewise, the SED distance agrees well with that from *Gaia*. However, the SED values for the sdB are not reasonable and will be discussed in Section 4.3.

## 4 DISCUSSION

K2 data have provided new insights into previously known sdBV stars discovered from ground-based photometry. For seismological studies, the nearly continuous, single-instrument observations provide data sets currently unmatched from the ground. These can be very useful for detecting features that can identify pulsation modes, determine physical properties (rotation and compositional discontinuities), and constrain structure models.

### 4.1 UY Sex

Prior to K2 observations, UY Sex had been observed during at least three different campaigns, including a multisite one. At best, 18 periodicities were observed during those campaigns, while we detected 97 periodicities from 80 d of K2 observations. While many of the periodicities could not be associated with pulsation modes, those that could be indicate p-mode overtone spacings in rough agreement with model predictions. The frequency splittings indicate a rotation period of 24.6 ± 3.5 d, which is more than double that found by Kilkenny et al. (2002b) and similar to that found in other sdBV stars (table 1 of Reed et al. 2018). UY Sex is relatively bright for K2-observed sdBV stars, and so the lack of g-mode periodicities indicates that either they are not excited at all in UY Sex or their amplitudes are exceptionally low.

Interestingly, UY Sex has some oscillations consistent with having stochastic properties. This would be similar to the other hot sdBV stars PG 0048+091, PG 1315−123 (Reed et al. 2019), and KIC 2991276 (Østensen et al. 2014), while V1405 Ori does not, though it has a similar temperature. This list of sdBV stars containing some oscillations with stochastic properties is likely incomplete as we suspect that there are more in publications that previously have not been identified. While their contribution may be small, their source could be of interest for pulsation stability calculations.

### 4.2 V1405 Ori

Discovered to be a p-mode sdBV star by Koen et al. (1999) and a reflection-effect binary by Reed et al. (2010), the vastly superior K2 observations show V1405 Ori to be a hybrid pulsator. Similar to UY Sex, many of the p-mode periodicities could not be identified. Those that could indicate an overtone spacing roughly in agreement with model predictions.

Our FT of K2 observations provides a very accurate binary period of 0.398023 ± 0.000003 d. This puts V1405 Ori in an interesting position between those sdBV stars that are tidally locked and have binary periods under a few hours and those with binary periods near half a day or longer but with subsynchronous rotations several days longer. V1405 Ori has a binary period just longer than KL UMa, and like that star (Reed et al. 2012), multiplets indicate an envelope rotation period just slightly longer than the binary period, indicating that it is close to but not quite synchronized. And yet, as is becoming commonplace with sdB pulsators, the sdB+dM binary PHL 457, which has an orbital period of 0.312 d, very similar to V1405 Ori, rotates subsynchronously with a period of 4.6 d for the interior and 2.5 d for the envelope (Baran et al. 2019).

While only a marginal detection, g-mode multiplets indicate an interior rotation period around 4 d. This would make V1405 Ori another radially differential rotator like KIC 3527751 (Foster et al. 2015) and PG 0048+091 (Reed et al. 2019), which all rotate more slowly in the core. This is contradictory to predictions, which

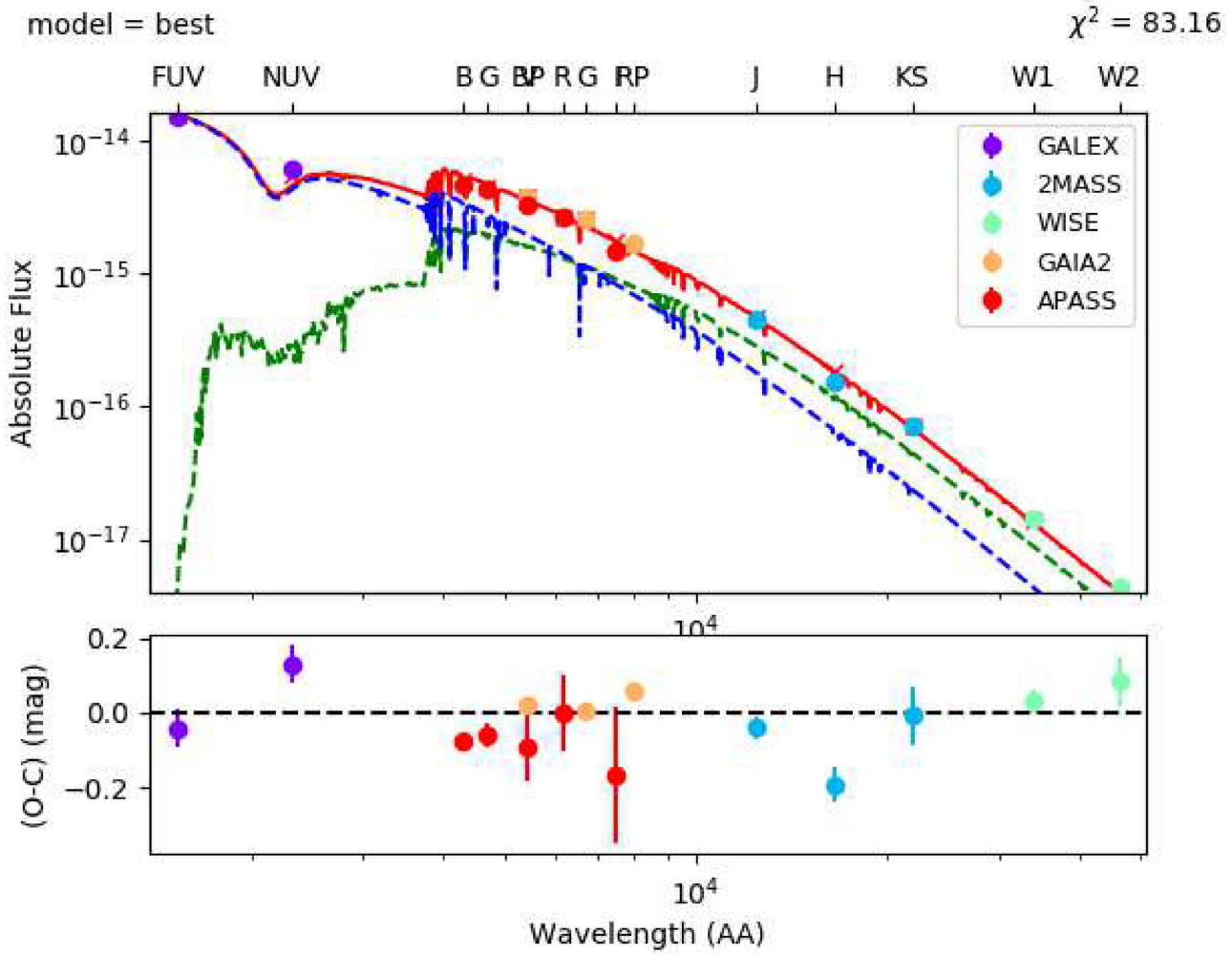


**Figure 13.** Spectral energy distribution for V1405 Ori. In the top panel, the blue dashed line is the sdB model, the green dashed line the MS model, and the solid red line is the combined model flux for case [a] of Table 7.

anticipated rapidly rotating cores decoupled from the envelope (Kawaler & Hostler 2005).

V1405 Ori has three frequencies very close to harmonics of the orbital frequency. There are no orbital overtones observed above the third overtone, yet these are not the highest amplitude frequencies. Two of them appear on asymptotic sequences and so the proximity of a natural frequency to an orbital overtone might drive them to observable levels. fN is not near an asymptotic sequence and so we forward the idea that one or more of these could be forced oscillations due to binarity. An asymmetry of forces from the binary on the sdB star would be required and the most likely candidate would be a slight ellipticity in the orbit. We do not have data required to investigate any orbital features and so leave it as one of V1405 Ori's unanswered questions for further investigation.

Another interesting feature is the seeming lack of $\ell \leq 2$ g modes. 16 of the 19 frequencies can be associated with $\ell = 3$ or 4 modes via asymptotic period spacings and the three others can be associated with frequency splittings of asymptotic members. As such, there are no available periodicities to be identified as $\ell \leq 2$. As V1405 Ori is one of the faster rotating g-mode sdBV stars, it is possible that mode selection is affected by rotation, suppressing the lowest degree modes, perhaps like those observed in $\delta$ Scuti (Solano & Fernley 1997) or $\beta$ Cepheid (Telting et al. 2006) stars. In both cases, those are p-mode pulsations, while for V1405 Ori, it is for g-mode pulsations. Unfortunately, V1405 Ori cannot really be compared to similarly rotating sdBV stars. No g modes have been detected in KL UMa and PG 0048+091 has a 4-d period for the envelope but a 16-d rotation period for the interior (Reed et al. 2019), making it much longer than V1405 Ori's. We note that in fig. 6 of Bloemen et al. (2014), their models predict that low-degree g modes are not excited until very late in horizontal branch evolution for stars of similar temperature but assuming a canonical core mass near 0.46 $M_\odot$ (see Xiong et al. 2017). As we cannot constrain the mass, it is certainly a possibility that the differing period spacings are indicative of a non-canonical core mass.

### 4.3 Issues with masses

With *Gaia* parallaxes becoming available, an extremely important constraint could be masses, which one could hope to correlate with g-mode period spacings. However, our results and other published results cast significant doubt on masses that were derived using a combination of spectroscopy, SED, and parallax measurements. Kilkenny, Worters & Lynas-Gray (2019) report six masses using a combination of spectroscopy and *Gaia* parallaxes and all their masses are lower than canonical, three significantly so. Baran et al. (2019) report spectroscopic, SED, and *Gaia* parallaxes for two sdBV

stars and derive masses that are significantly lower than canonical. In Baran et al. (2019), it is noted that 'since the error on the surface gravity is likely underestimated, the real error on the mass of the sdB component is also underestimated', which takes them to the conclusion 'that the mass of the sdB star cannot be constrained very well by this means'.

Our own SED fit results in a mass for UY Sex of $0.64 \pm^{+0.08}_{-0.07}$ $M_{\odot}$, which is inconsistent with spectroscopic values. The evolutionary tracks of Bloemen et al. (2014, their fig. 4) do not go as massive as $0.64\,M_{\odot}$, but our spectroscopic values place UY Sex on the track for $0.47\,M_{\odot}$, or less if more evolved. Also in contrast to our SED-determined mass, Charpinet et al. (2003) found $M = 0.490 \pm 0.014\,M_{\odot}$ from a seismic model. The solution for V1405 Ori is also problematic, with a radius that is likely too small and a mass of $0.28 \pm 0.10\,M_{\odot}$ that is far too low for a core He-fusing star. There is little doubt that high reddening and varying luminosity from the reflection effect are adversely affecting those results. However, the end result is that we likely fail to place useful constraints on these masses, even though we have a significant combination of tools at our disposal. V1405 Ori has a binary companion that produces unsolved geometric effects including temporally unresolved reflection luminosity variations, but UY Sex appears as a single star and so its unusual mass questions the procedure in its entirety. The reasons for these mismatches are beyond the scope of this paper, but we note this as an extremely important constraint and strongly encourage its investigation.

## ACKNOWLEDGEMENTS

MY and AS were funded by the Missouri Space Grant, which is funded by NASA. ASB gratefully acknowledges financial support from the Polish National Science Center under project no. UMO-2017/26/E/ST9/00703 and UMO-2017/25/B ST9/02218. This paper includes data obtained by the *Kepler* mission. Funding for the *Kepler* mission is provided by the NASA Science Mission directorate. Data presented in this paper were obtained from the Mikulski Archive for Space Telescopes (MAST). STScI is operated by the Association of Universities for Research in Astronomy, Inc., under NASA contract NAS5-26555. Support for MAST for non-*HST* data is provided by the NASA Office of Space Science via grant NNX13AC07G and by other grants and contracts.

The spectroscopic observations used in this work were obtained with the Nordic Optical Telescope at the Observatorio del Roque de los Muchachos and operated jointly by Denmark, Finland, Iceland, Norway, and Sweden.

## REFERENCES

Bailer-Jones C. A. L., Rybizki J., Fouesneau M., Mantelet G., Andrae R., 2018, AJ, 156, 58
Baran A., Pigulski A., O'Toole S. J., 2008, MNRAS, 385, 255
Baran A. S. et al., 2012, MNRAS, 424, 2686
Baran A. S. et al., 2018, MNRAS, 481, 2721
Baran A. S., Reed M. D., Østensen R. H., Telting J. H., Jeffery C. S., 2017, A&A, 597, A95
Baran A. S., Telting J. H., Jeffery C. S., Østensen R. H., Vos J., Reed M. D., Vućković M., 2019, MNRAS, 489, 1556
Bevington P. R., Robinson D. K., 2003, Data Reduction and Error Analysis for the Physical Sciences. McGraw-Hill, Boston, MA
Billères M., Fontaine G., Brassard P., Charpinet S., Liebert J., Saffer R. A., Vauclair G., 1997, ApJ, 487, L81
Bloemen S., Hu H., Aerts C., Dupret M. A., Østensen R. H., Degroote P., Müller-Ringat E., Rauch T., 2014, A&A, 569, A123
Charpinet S., Fontaine G., Brassard P., 2003, in de Martino D., Silvotti R., Solheim J. E., Kalytis R., eds, NATO ASIB Proc. 105, White Dwarfs Vol. 105, Fundamental Parameters of sdB Pulsators from Asteroseismology. Kluwer Academic Publishers, Dordrecht, p. 69
Charpinet S., Fontaine G., Brassard P., Chayer P., Rogers F. J., Iglesias C. A., Dorman B., 1997, ApJL, 483, L123
Charpinet S., Fontaine G., Brassard P., Dorman B., 2000, ApJS, 131, 223
Charpinet S., Fontaine G., Brassard P., Dorman B., 2002, ApJS, 139, 487
Constantino T., Campbell S., Christensen-Dalsgaard J., Lattanzio J., Stello D., 2015, MNRAS, 452, 123
Cutri R. M. et al., 2012, VizieR Online Data Catalog, 2311
Djupvik A. A., Andersen J., 2010, Astrophys. Space Sci. Proc., 14, 211
Evans D. W. et al., 2018, A&A, 616, A4
Foreman-Mackey D., Hogg D. W., Lang D., Goodman J., 2013, PASP, 125, 306
Foster H. M., Reed M. D., Telting J. H., Østensen R. H., Baran A. S., 2015, ApJ, 805, 94
Gaia Collaboration et al., 2018, A&A, 616, A1
Gaia Collaboration et al., 2016, A&A, 595, A1
Geier S. et al., 2014, A&A, 562, A95
Ghasemi H., Moravveji E., Aerts C., Safari H., Vućković M., 2017, MNRAS, 465, 1518
Green E. M. et al., 2003, ApJL, 583, L31
Heber U., 2016, PASP, 128, 082001
Heber U., Reid I. N., Werner K., 1999, A&A, 348, L25
Henden A. A., Levine S., Terrell D., Welch D. L., 2015, American Astronomical Society Meeting Abstracts, #225 . p. 336.16
Jeffery C. S. et al., 2017, MNRAS, 465, 3101
Kawaler S. D., Hostler S. R., 2005, ApJ, 621, 432
Kern J. W., Reed M. D., Baran A. S., Telting J. H., Østensen R. H., 2018, MNRAS, 474, 4709
Ketzer L., Reed M. D., Baran A. S., Németh P., Telting J. H., Østensen R. H., Jeffery C. S., 2017, MNRAS, 467, 461
Kilkenny D. et al., 2002a, MNRAS, 331, 399
Kilkenny D. et al., 2002b, MNRAS, 331, 399
Kilkenny D., Koen C., O'Donoghue D., Stobie R. S., 1997, MNRAS, 285, 640
Kilkenny D., Worters H. L., Lynas-Gray A. E., 2019, MNRAS, 485, 4330
Koen C., O'Donoghue D., Kilkenny D., Stobie R. S., Saffer R. A., 1999, MNRAS, 306, 213
Kurucz R. L., 1979, ApJS, 40, 1
Lallement R., Babusiaux C., Vergely J. L., Katz D., Arenou F., Valette B., Hottier C., Capitanio L., 2019, A&A, 625, A135
Ledoux P., 1951, ApJ, 114, 373
O'Donoghue D., Koen C., Lynas-Gray A. E., Kilkenny D., van Wyk F., 1998, MNRAS, 296, 306
Østensen R. H., Reed M. D., Baran A. S., Telting J. H., 2014, A&A, 564, L14
Østensen R. H. et al., 2010, MNRAS, 409, 1470
Østensen R. H. et al., 2011, MNRAS, 414, 2860
Østensen R. H., Telting J. H., Reed M. D., Baran A. S., Nemeth P., Kiaeerad F., 2014, A&A, 569, A15
Pesnell W. D., 1985, ApJ, 292, 238
Reed M. D. et al., 2004, MNRAS, 348, 1164
Reed M. D. et al., 2010, Ap&SS, 329, 83
Reed M. D. et al., 2011, MNRAS, 414, 2885
Reed M. D. et al., 2016, MNRAS, 458, 1417
Reed M. D. et al., 2018, MNRAS, 474, 5186
Reed M. D. et al., 2018, Open Astron., 27, 157
Reed M. D. et al., 2012, in Kilkenny D., Jeffery C. S., Koen C., eds, ASP Conf. Ser. Vol. 452, Multicolor Photometry and Time-resolved Spectroscopy of Two sdBV Stars. Astron. Soc. Pac., San Francisco, p. 193
Riello M. et al., 2018, A&A, 626, A3
Reed M. D. et al., 2019, MNRAS, 483, 2282
Silvotti R., Uzundag M., Baran A. S., Østensen R. H., Telting J. H., Heber U., Reed M. D., Vŭcković M., 2019, MNRAS, 489, 4791
Skrutskie M. F. et al., 2006, AstronJ, 131, 1163

Solano E., Fernley J., 1997, A&AS, 122, 131
Telting J. H., Østensen R. H., Oreiro R., Reed M., Farris L., O'Toole S., Aerts C., 2012, in Kilkenny D., Jeffery C. S., Koen C., eds, ASP Conf. Ser. Vol. 452, Orbits of Hot Subdwarf Binaries in the Kepler Field. Astron. Soc. Pac., San Francisco, p. 147
Telting J. H., Schrijvers C., Ilyin I. V., Uytterhoeven K., De Ridder J., Aerts C., Henrichs H. F., 2006, A&A, 452, 945
Vos J., Østensen R. H., Németh P., Green E. M., Heber U., Van Winckel H., 2013, A&A, 559, A54 (Paper II)
Vos J., Østensen R. H., Vučković M., Telting J. H., 2017, A&A, 605, A109
Werner K., Deetjen J. L., Dreizler S., Nagel T., Rauch T., Schuh S. L., 2003, in Hubeny I., Mihalas D., Werner K., eds, ASP Conf. Ser. Vol. 288, Model Photospheres with Accelerated Lambda Iteration. Astron. Soc. Pac., San Francisco, p. 31
Xiong H., Chen X., Podsiadlowski P., Li Y., Han Z., 2017, A&A, 599, A54

This paper has been typeset from a TEX/LATEX file prepared by the author.